NASA Technical Memorandum 107621

Further Buffeting Tests in a Cryogenic Wind Tunnel

D. G. Mabey, R. P. Boyden,
and W. G. Johnson, Jr.

(NASA-TM-107621) FURTHER BUFFETING TESTS IN A CRYOGENIC WIND TUNNEL (NASA) 55 p

N93-11610

Unclas

G3/02 0126288

SEPTEMBER 1992

National Aeronautics and
Space Administration

Langley Research Center
Hampton, Virginia 23665-5225

LIST OF CONTENTS

FURTHER BUFFETING TESTS IN A CRYOGENIC WIND TUNNEL

by

D. G. Mabey (RAE Bedford)
R. P. Boyden (NASA Langley)
W. G. Johnson, Jr. (NASA Langley)

SUMMARY

Further measurements of buffeting, using wing-root strain gauges, were made in the NASA Langley 0.3m Cryogenic Wind Tunnel to refine techniques which will be used in larger cryogenic facilities such as the United States National Transonic Facility (NTF) and the European Transonic Wind Tunnel (ETW). The questions addressed included the relative importance of variations in frequency parameter and Reynolds number, the choice of model material (considering both stiffness and damping) and the effects of static aeroelastic distortion.

The main series of tests was made on three half models of slender 65° delta wings with a sharp leading edge. The three delta wings had the same planform but widely differing bending stiffnesses and frequencies (obtained by varying both the material and the thickness of the wings). It was known that the flow on this configuration would be insensitive to variations in Reynolds number.

Additional tests were made on one unswept half-wing of aspect ratio 1.5 with an NPL 9510 aerofoil section, known to be sensitive to variations in Reynolds number at transonic speeds. For brevity the test March numbers were restricted to $M = 0.21$ and 0.35 for the delta wings and to $M = 0.30$ for the unswept wing.

1. INTRODUCTION

The accurate prediction during the design stage of the onset and severity of wing buffeting likely to be met in flight is of great importance for both transport and combat aircraft[1]. Hence there is considerable interest in developing and refining experimental techniques that can be used with confidence during model tests in wind tunnels.

The dynamic method of measuring wing buffeting on models and aircraft using root-strain gauges was suggested for by Huston[2]. Subsequently it was developed by Jones[3] and others for use in conventional wind tunnels and in flight. In some preliminary tests, Boyden and Johnson[4] showed conclusively that this technique could be employed also in cryogenic wind tunnels; also, with such a facility, effects on buffeting due to static aeroelastic distortion and variations in Reynolds number could be distinguished. However, some additional tests were judged necessary to clarify some outstanding issues.

Three principal questions were addressed. The first was to confirm that the buffet excitation parameter (derived as specified in Ref. 1) could be measured in cryogenic facilities. The buffet excitation parameter depends on the total damping (aerodynamic plus structural) in the bending mode as well as on the mode shape and generalized mass (*cf* discussion of equation (3)). Hence this question implies consideration of the variation of both aerodynamic and structural damping at cryogenic conditions. Previous experience in a conventional wind tunnel suggests[1] that an ideal model would provide a high level of aerodynamic damping, and a low level of structural damping because this would facilitate extrapolation of wind-tunnel measurements to flight. The present tests imply that appropriate aerodynamic and structural levels can be provided on aluminium or steel models in a cryogenic wind tunnel (although no steel models were tested).

The second question relates to the importance of the frequency parameter, $n = f\bar{\bar{c}}/U$. For many wings the buffet excitation parameter varies slowly with the frequency parameter so that this does not need to be presented precisely. However, for a slender delta wing after vortex breakdown, the buffet excitation parameter is sensitive to the frequency parameter so that flight full-scale values must be represented precisely. This was confirmed here by tests on three half models of slender delta wings with the same planform but with widely differing bending stiffnesses and frequencies. The flow on these slender wings was known to be insensitive to variations in Reynolds number[5].

The third question relates to the suitability of carbon fibre composite materials for models to be tested in cryogenic wind tunnels. Models made in carbon fibre have given encouraging results for oscillatory tests in conventional wind tunnels because of their stiffness and lightness[6,7]. Accordingly two of the delta wings were made in carbon fibre. The measurements show that although carbon fibre is a suitable material for models to be tested in cryogenic wind tunnels, care is required in laying up the fibres to achieve the required bending and torsional stiffnesses. The aerodynamic and structural damping provided by the carbon fibre models is satisfactory for buffeting tests. These comparative tests of the delta wings also provide information about the effects of static aeroelastic distortion.

This second series of tests is described in the present paper and definitive recommendations are made for future test techniques. This Memorandum stems from a joint research

project between NASA Langley and RAE Bedford, originally suggested in a lecture at Langley[8].

2. EXPERIMENTAL DETAILS

In general the second series of tests had much in common with the original tests[4]. Hence for brevity only significant changes are recorded.

2.1 Wind tunnels and test conditions

For the original tests[4] the tunnel two-dimensional section was used (breadth = 203 mm and height = 610 mm, Fig. 1a): this section had a slotted floor and roof with solid sidewalls. For the present tests a two-dimensional closed adaptive-wall test section was used (breadth = 330 mm and height = 330 mm, Fig. 1b). The top and bottom adaptive walls were kept straight with linear divergence for these tests (*ie* the walls were used in a nonadaptive mode). This gave a constant Mach number through the test section without a model. Only low Mach numbers ($M = 0.35$ and 0.21) were used for these tests, which were made at total pressures varying between $p_t = 1.2$ bar and 4.8 bar and total temperatures varying between 300 K and 110 K.

2.2 Choice of models

Two radically different types of half model were tested (Fig. 2). The three 65° delta wings (Fig. 2a and Table 1) had a chamfer providing a sharp leading edge. No attempt was made to fix transition because of the separations expected from the chamferred leading edge. The aluminium delta was the one tested previously[4]. It was 5.1 mm thick and had a first bending frequency of 480 Hz. The other two delta wings were made in carbon fibre. One of these models had an identical geometry to that of the aluminium delta. However, because of the combined effects of the lower density and a small increase in Young's Modulus, the first bending frequency increased to 650 Hz. The other carbon fibre delta has a reduced thickness of only 2.5 mm and hence a lower first bending frequency of 360 Hz. Thus with these three models, for fixed aerodynamic conditions, both the static bending stiffness and the frequency parameter in bending could be varied over wide ranges.

The bending and torsional frequencies of the three delta models are compared in Table 1. The bending frequencies, taken in conjunction with the wing densities given in Appendix B, imply that the bending deflections due to a given static load would be a maximum for the thin carbon fibre wing but smaller and about the same for the thick carbon fibre and the aluminium wings. This is consistent with the relative bending moduli inferred from the deflection measurements, although smaller bending deflections were expected for the thick carbon fibre wing (Table 1). In contrast, the torsional frequencies imply that the torsional modulus for the thick carbon fibre wing is only 0.74 relative to that of the aluminium wing, whereas that for the thin carbon fibre wing is 2.54. The relative static torsional stiffnesses inferred were thus 0.74 and 0.30 for the thick and thin carbon fibre wings. However, the static twist due to torsion was not measured. Possibly on these delta wings static aeroelastic distortion would represent primarily increased wing twist near the tip for both carbon fibre composite deltas relative to the aluminium delta. Carbon fibre composite (unlike aluminium and steel) is not an isotropic material and differing ratios of torsional and bending stiffness can be achieved depending on how the fibres are aligned. This can be utilized in wing design.

The single unswept half-wing (Fig. 2b) was made of aluminium and was tested previously[4] with free transition. During the present tests transition was fixed by a roughness band of micro-beads with a nominal diameter of 0.048 mm extending from $x/c = 5\%$ to $x/c = 7.5\%$ on both the upper and lower surfaces of the wing. The wing first bending frequency was 270 Hz, as in the previous tests.

All four models were mounted on the half-model turntable. This was made of the same type of the aluminium alloy (7075-T6) as used for the aluminium wings "to minimize the effects of thermal expansion and contraction over the range of test temperatures in order to provide a model mounting as rigid as possible to keep the structural damping to a minimum"[4]. However, use of this turntable precluded the measurement of the overall force coefficients, such as lift (C_L), pitching moment (C_M), and drag (C_D) which could have been measured with a half-model balance. These force measurements would have been particularly useful when attempting to infer the type of flow separations on the unswept wing. They would also have allowed a direct check on the lift on the delta wings given by equation (4). In the absence of measurements of the overall lift and normal force on the wings, the wing static bending-moment coefficients (derived from the root strain gauges: *cf* equation (1) in section 2.5) become of considerable interest. However, some of these measurements for the unswept wing were subject to significant zero errors (*cf* discussion of Fig. 13). Hence some refinement in test technique appears desirable.

2.3 Instrumentation

The buffet data acquisition system used for these tests is a two-channel integrated unit designed by personnel of the Langley Instrument Research Division. Each channel of the buffet system includes switch-selectable gain settings from 200 to 20000, an active low-pass filter, a root-mean-square converter, and an integration circuit. It may be operated in either an ac or a dc mode. The dc mode is normally used for wind-off calibration of the bending-moment strain gauge by application of known moments to the wing with weights. The dc mode is also utilized to measure the wind-on, steady-state, root bending moments of the wings. In the ac mode, the steady or dc voltages are automatically suppressed. The system averages the root-mean-square values of the unsteady voltage signals from the bending-moment strain gauge by integrating the signal for a time interval which is preselected from 1 to 99 s. For this test, an integration time of 20 s was used. The two-pole, low-pass, active filter is mounted on plug-in boards and is used to limit the frequency content above the range of interest which is the first bending frequency. The unsteady bending-moment signal was recorded on a magnetic tape recorder for later off-line analysis.

2.4 Test procedure

Before the actual wind-tunnel test, the models were loaded statically while in an environmental chamber in order to determine the effect of the temperature range on the sensitivity of the root bending-moment strain gauges. The variation in sensitivity with temperature was found to be linear for all of the wings over the range from 300 K to 110 K. Over this temperature range, the sensitivity for the two aluminium wings increased about 22% due to a poor match in the type of strain gauges used. For the two carbon-fibre wings the sensitivity increased by about 2%. The strain-gauge sensitivity for each model was corrected as a function of temperature in the data reduction process.

After the wind tunnel had reached the required test conditions and the angle of attack had been set, the gain of the buffet measuring system was adjusted to maximize the output of the unsteady wing-root bending-moment signal without overloading the instrumentation. This signal was monitored with an oscilloscope and a recording oscillograph for amplifier overload and for the allowable input range for the analogue tape recorder. The unsteady bending-moment signal was then integrated for the 20 s time interval chosen for this test and then the integrated voltage and amplifier gain setting were recorded on the tunnel data-acquisition system. Afterwards, a 45 s segment of the unsteady signal was recorded on magnetic tape for later analysis. Then, the steady root bending-moment signal was measured and recorded on the tunnel data-acquisition system. For on-line display purposes, both the steady and the dynamic wing-root bending-moment coefficients were also computed and plotted on a desk top micro-computer with an attached plotter.

The analogue signals recorded on magnetic tape were later digitized at 2500 samples/s for off-line analysis. About 43 s of data at each selected test point were processed by digital analysis techniques. Measurements of the total damping ratio were made from a least-squares fit of the decay of the envelopes of the autocorrelation function[9]. The frequency of oscillation was determined from the average time between peaks of the autocorrelation function.

2.5 Presentation of results

The static and dynamic measurements on all four models are presented as coefficients defined below.

Static bending-moment coefficient:

$$\overline{C}_B = \frac{\text{steady bending moment}}{qS\overline{\overline{c}}}, \tag{1}$$

where q is the kinetic pressure, S is the wing area, and $\overline{\overline{c}}$ the aerodynamic mean chord. Estimates of $\overline{C}_B$ for the delta and unswept wings are given in Appendix A.

Dynamic bending-moment coefficient:

$$C_B = \frac{\text{rms dynamic bending moment}}{qS\overline{\overline{c}}}. \tag{2}$$

The static calibration factor used in equation (1) to obtain steady bending moments from steady strain gauge readings is assumed to apply to the conversion of dynamic strain gauge readings to the dynamic bending moment.

Although the coefficient C_B is adequate for a quick assessment of the unsteady measurements, it is not appropriate to scaling to other structures. This can be achieved only if the dynamic measurements are expressed in terms of the buffet excitation parameter in the mode excited, defined[1] as:

$$\sqrt{nG(n)} = \frac{2}{\sqrt{\pi}}\frac{m\ddot{z}}{qS}\zeta^{1/2}, \tag{3}$$

where m = generalized mass in mode with respect to motion at tip,
$\ddot{z}$ = rms of fluctuating tip acceleration in mode,
ζ = total damping—as ratio to critical damping,
and $n = f\overline{\overline{c}}/V$ is the frequency parameter.

Use of $\sqrt{nG(n)}$ would have required measurements of the generalized masses and the calibration factors between wing-tip accelerations and the wing-root strain signals for all four models and these were not available. Estimates of the total damping ratio for the delta wings are compared to the measurements in Appendix B.

3. RESULTS

3.1 Delta wings

3.1.1 General description of flow and buffeting characteristics. As a reference, it is helpful to recall the main features of the forces and flows (Fig. 3) on 65° delta wings of this type observed previously[5] in a variable density wind tunnel at ambient temperatures. These observations were made on a pair of identical wings (one made of steel and the other of magnesium, having widely differing values of Young's Modulus, E, but the same bending frequency) at $M = 0.35$ and 0.70, in a closed working section selected because of its low level of flow unsteadiness. It is important to note that there is no evidence of any effects due to static aeroelastic distortion (due to bending or torsion) within these measurements.

The variation of the normal force coefficient, C_N, with the angle of incidence, α, is linear for both wings from about 0° to 10° (Fig. 3a). The slope, $dC_N/d\alpha$, is close to the lift curve slope given by slender wing theory of:

$$\frac{dC_L}{d\alpha} = \frac{\pi}{2}A. \tag{4}$$

From $\alpha = 10°$ to 20° significant non-linear lift develops due to the formation of leading edge vortices (*eg* as shown for $\alpha = 20°$ in Fig. 3b). Fig. 3c shows that the measurements of the buffet excitation parameter at the fixed frequency parameter $f\overline{\overline{c}}/U = 0.34$ are the same on both wings despite the widely varying values of generalized mass, tip amplitude and damping. Formation of the tightly rolled vortices produces a low level of buffeting from $\alpha = 5°$ to 15°. Above $\alpha = 18°$ there is a progressive increase in the buffet excitation parameter as vortex breakdown moves upstream and approaches the trailing edge. The light and moderate buffeting levels ($\sqrt{nG(n)} = 0.0075$ and 0.0150) are reached at $\alpha = 22°$ and 26°. Ref. 5 does not include any investigation of the effects of frequency parameter on the buffet excitation parameter at a constant angle of incidence above vortex breakdown. However the measurements of Ref. 4 suggest that above vortex breakdown there is a strong effect of the frequency parameter. This is consistent with Keating's unpublished measurements of the excitation spectrum on a slender wing BAC 221 model with vortex breakdown. These measurements are important and hence they are reproduced in Fig. 3d from Ref. 1. Although the geometry of the BAC 221 was appreciably different from a 65° delta wing, it is known that the flows on both wings are broadly comparable. Here the large increase in excitation from a frequency parameter, fc_0/V, from 0.9 to 1.4 observed in Ref. 4 is consistent with the increase in response. We shall see that similar characteristics are found in the present tests.

3.1.2 Tests at ambient temperatures. Tests at ambient total temperature at two different total pressures on the present three delta wings at $M = 0.35$ (Fig. 4) provide an interesting comparison with the original measurements in a conventional wind tunnel (Ref. 5 and Fig. 3). During these more recent tests at constant total temperature, the Reynolds number and kinetic pressure increase monotonically with the total pressure, so that for each model the effects of any changes due to Reynolds number and aeroelastic distortion are combined, as in a conventional variable-density wind tunnel and cannot be separated. (However, the subsequent tests will show how the unique capability of the cryogenic tunnel allows the separate effects to be identified.) On each particular model the frequency parameter, n, is constant because both the frequency and the velocity are constant for this mode of testing.

For the aluminium wing (Fig. 4a) the static bending-moment coefficients, $\overline{C}_B$, are identical up to $\alpha = 18°$ for the two pressures, which suggests that the combined effects of variations in Reynolds number and static aeroelastic distortion are negligible. When account is taken of the displacement of the gauge centre from the model center line (see discussion in Appendix A) the slope, $d\overline{C}_B/d\alpha$, is somewhat lower than would be expected from the previous tests[5] (which were consistent with the lift given by equation (4)). For angles of incidence above $\alpha = 18°$, vortex breakdown approaches the trailing edge and the static bending-moment coefficients are appreciably lower at the higher total pressure. We shall see later (*cf* discussion of Fig. 5) that this reduction is due primarily to static aeroelastic distortion, rather than to the effect of Reynolds number (*cf* discussion of Fig. 6). The minima in $\overline{C}_B$ (at 20° and 22° at the lower and higher total pressures) are closely associated with vortex breakdown.

For the unsteady measurements the frequency parameter is $n = 0.55$ and the increases in C_B above $\alpha = 18°$ and 20° at the lower and higher total pressures clearly indicate the approach of vortex breakdown to the trailing edge. Over the whole incidence range the C_B levels are appreciably lower at the higher total pressure. This is because the total damping is higher at the higher pressures ($\zeta = 0.025$ compared to $\zeta = 0.009$) due to the increase in aerodynamic damping. Thus the 60% reduction in C_B may be explained by equations (2) and (3) under the assumption that there are no static aeroelastic distortion effects and/or scale effects on $\sqrt{nG(n)}$.

For the thick carbon fibre delta (Fig. 4b) the static bending-moment coefficients are identical at both total pressures up to $\alpha = 24°$. This might be thought to imply that the combined effects of static aeroelastic distortion and Reynolds number are negligible over a wide incidence range. However the slope $d\overline{C}_B/d\alpha$ from $\alpha = 0°$ to 18° is 10% lower than for the nominally identical aluminium delta. This large change implies that the lift must be reduced, possibly due to the greater twist of the carbon fibre model towards the tip. Possible causes are discussed in Appendix C. For this model the static bending-moment coefficient above $\alpha = 24°$ is a little higher at the higher total pressure than at the lower total pressure. This anomaly is inconsistent with the corresponding measurements on the other two wings (*cf* Figs. 4a and c). For the unsteady measurements the frequency parameter is $n = 0.73$ and C_B is again lower at the higher total pressure (because of an increase in total damping from $\zeta = 0.010$ to $\zeta = 0.026$).

For the thin carbon-fibre delta (Fig. 4c) the static bending-moment coefficients are identical at both total pressures up to $\alpha = 8°$, with a further reduction in slope compared to that of the thick carbon fibre delta. Above $\alpha = 8°$, the C_B values are appreciably lower at

the higher total pressure, consistent with large aeroelastic effects on this flexible model. For the unsteady measurements the frequency parameter is $n = 0.41$ and C_B is again lower at the higher total pressure. Note that for this flexible model the C_B levels are much smaller than for the other two models, again due to the greatly increased aerodynamic damping. (The total damping values are $\zeta = 0.020$ and 0.060 at the lower and higher kinetic pressures.)

3.1.3 Tests at constant Reynolds number and Mach number. The unique features of a cryogenic wind tunnel were exploited to demonstrate the effects of static aeroelastic distortion on the steady measurements, independent of any variations due to Reynolds number. This was achieved by tests for a constant Reynolds number of $R = 4.8 \times 10^6$ at $M = 0.35$, obtained from two different combinations of total temperature and total pressure, giving widely different values of kinetic pressure (Fig. 5). On any particular delta, for this mode of testing, the frequency parameter is higher at the lower total temperature because of the lower velocity.

For the aluminium delta (Fig. 5a), the static bending-moment coefficients, $\overline{C}_B$, are identical up to $\alpha = 18°$, which suggests that the effects of static aeroelastic distortion are negligible with a small, tightly rolled vortex. The slope, $d\overline{C}_B/d\alpha$, is identical with that measured at ambient conditions, which deliberately cover the same range of kinetic pressure (*cf* Fig. 4a). Above $\alpha = 18°$ vortex breakdwon approaches the trailing edge, with a clear minimum at $\alpha = 22°$. Above $\alpha = 22°$ the static bending-moment coefficients are appreciably lower at the higher kinetic pressure, indicating a strong influence of aeroelastic distortion. This radical change is almost the same as that measured at ambient conditions (*cf* Fig. 4a). This provides an indication that in conventional wind tunnels, effects of static aeroelastic distortion could have been confused with, or even attributed to, variations in Reynolds number. For the unsteady measurements the signals are small below $\alpha = 18°$. Above $\alpha - 18°$ the buffeting increases as vortex breakdown approaches the trailing edge. The much lower values of C_B at the higher kinetic pressure are due to the combined effects of the change in aerodynamic damping and the change in excitation. The first effect is due to the increased aerodynamic damping (proportional to the product ρV) which should be 2.4 times higher at the higher kinetic pressure. However, this only increases the total damping, ζ, from about $\zeta = 0.020$ to 0.025 which would make the response (represented by C_B) about 10% smaller according to equation (3). This is only a relatively small effect. The second effect is due to the change in excitation due to the changes in frequency parameter and, to a lesser extent, to changes due to static aeroelastic distortion (associated with the changed values of $\overline{C}_B$). For the higher kinetic pressure the frequency parameter is lower and this makes the excitation lower. This is consistent with the measurements of the excitation spectrum shown in Fig. 3d.

For the thick carbon fibre delta (Fig. 5b) the static bending-moment coefficients are identical up to about $\alpha = 12°$, which might be thought to imply that the effects of static aeroelastic distortion are small over this range. However, the slope, $dC_B/d\alpha$, is 10% lower than that for the nominally identical aluminium delta. For this model above $\alpha = 16°$ the static bending-moment coefficient is appreciably lower at the higher kinetic pressure due static aeroelastic distortion, consistent with the measurements on the aluminium delta. The unsteady measurements are similar in character to those on the aluminium wing, the C_B levels above $\alpha = 20°$ again being much lower at the higher kinetic pressures. Again this is due primarily to the lower excitation at the lower frequency parameter. In addition the total damping on this model varies from about $\zeta = 0.012$ at the lower kinetic pressure to

$\zeta = 0.025$ at the higher kinetic pressure. This increase in damping would make the response (represented by C_B) about 30% smaller according to equation (3). This is a significant effect, quite apart from that due to the change in frequency parameter.

For the thin carbon fibre delta (Fig. 5c), the static bending-moment coefficients are identical up to $\alpha = 8°$ although with a further reduction in slope compared to that of the thick carbon fibre wing. Between $\alpha = 8°$ and 24° the C_B values are appreciably lower at the higher kinetic pressure showing a large effect of static aeroelastic distortion, consistent with that observed at ambient conditions (*cf* Fig. 4c). For $\alpha = 28°$ and 30° the C_B values are higher at the higher total pressure. This minor anomaly has not yet been explained and is inconsistent with the measurements on the other two wings. For the unsteady measurements, C_B is lower again at the higher kinetic pressure, due primarily to the lower excitation at the lower frequency parameter. In addition the total damping on this model varies from about $\zeta = 0.03$ to 0.06, which would make the response (represented by C_B) about 30% smaller at the higher kinetic pressure.

3.1.4 Tests at constant kinetic pressure and Mach number. The unique features of a cryogenic wind tunnel were exploited to demonstrate the effects of variations in Reynolds number at constant kinetic pressure. This can be achieved by testing at a fixed total pressure and Mach number ($M = 0.35$) but varying total temperature (Fig. 6). On a particular model, for this mode of testing (provided the elastic stiffness and frequency are invariant with temperature), the frequency parameter is higher at the lower total temperature because of the lower velocity, as in the investigation of the effects of static aeroelastic distortion (*cf* section 3.1.3 above). The aerodynamic damping is also higher at the lower total temperature, as shown previously[8].

For the aluminium delta (Fig. 6a) there are no scale effects on the static bending-moment coefficients over the incidence range from $\alpha = 0°$ to 18°. However, the angle of incidence for the minimum in $\overline{C}_B$ increases from $\alpha = 20°$ at $R = 1.2 \times 10^6$ to $\alpha = 22°$ for $R = 4.8 \times 10^6$. This is a precise indication of a genuine scale effect. This effect was observed also in Fig. 4a, but there it could not be attributed entirely to the change in Reynolds number because of the simultaneous variation in the kinetic pressure, which could have caused aeroelastic distortion. For the incidence range $\alpha \geq 24°$, there is a further important scale effect. Here the static bending-moment coefficients are appreciably higher at the higher Reynolds number. It is important to recall that in the corresponding tests at ambient total temperature (Fig. 4a), this genuine scale effect was completely hidden by the large opposite effect thought to be due to static aeroelastic distortion (Fig. 5a).

Inevitably the effect of the Reynolds number variation on the unsteady bending-moment coefficient is combined with the large effect of the associated change in frequency parameter and the small change in damping. Thus according to the unsteady measurements of Fig. 6a, the angle of incidence for vortex breakdown increases from about $\alpha = 20°$ at $R = 1.2 \times 10^6$ to $\alpha = 22°$ (or even $\alpha = 24°$) at $R = 4.8 \times 10^6$. However, the most interesting feature of these measurements is the much higher levels at $\alpha = 26°$ and 28° at the high frequency parameter associated with the higher Reynolds number. This variation with frequency parameter is consistent with the variation in local excitation shown in Fig. 3d. However, some of the much smaller increase at the lower Reynolds number is due to the lower level of total damping ($\zeta = 0.009$ at $R = 1.2 \times 10^6$ compared to $\zeta = 0.020$ at $R = 4.8 \times 10^6$).

The results for the thick carbon fibre delta (Fig. 6b) show the same general characteristics as the aluminium wing, although differing in significant details. Thus for the steady measurements there are no scale effects on the steady bending-moment coefficient over the reduced incidence range from $\alpha = 0°$ to $16°$. However, it is important to note that the slope, $d\overline{C}_B/d\alpha$, is about 10% lower than for the aluminium wing. For this delta there is also no minimum in $\overline{C}_B$ clearly marking vortex breakdown, again probably due to the larger distortion. However, above $\alpha = 18°$ the $\overline{C}_B$ values are appreciably higher at the higher Reynolds number, the change suggesting a larger scale effect than that observed on the aluminium delta. With regard to the unsteady bending-moment coefficient, the most interesting feature is the much higher levels of C_B from $\alpha = 24°$ to $28°$ at the higher Reynolds number. For this model all of this change can be attributed to the combined effects of the variations due to frequency parameter (thought to be large) and the variations due to Reynolds number (thought to be small). This is because for this model the total damping did not change significantly, being only about $\zeta = 0.011$ at both total temperatures. Presumably the expected small increase in aerodynamic damping at the lower total temperature is offset by a decrease in the structural damping. The absence of any large variation in structural damping coefficient with total temperature is an important result (albeit a negative one), particularly for the carbon fibre composite models. Further evidence for the absence of large variations in structural damping coefficient with total temperature for all models is provided in Appendix B.

All the results for the thin carbon fibre wing (Fig. 6c) are radically different in character from those for the other two wings. Thus for the steady bending-moment coefficient there are apparently no scale effects over the much wider incidence range from $\alpha = 0°$ to $22°$, although the slope is appreciably lower than for the thick carbon fibre wing. Above $\alpha = 22°$ there is a remarkable change in character, the $\overline{C}_B$ values now being lower at the higher Reynolds number. One tentative explanation for this major anomaly is that at the higher Reynolds number the higher lift developed distorts the wing and displaces the vortex inboard. This might reduce the static bending-moment coefficient, despite an increase in lift. Whatever the explanation, clearly there are major inconsistencies between the steady measurements on this model and the other two models. Again with regard to the unsteady measurements there are differences in character. The unsteady bending-moment coefficients are low at both Reynolds numbers, and vortex breakdown is not very clearly marked, even at the higher frequency parameter (the higher Reynolds number) where increased excitation would be expected. The total damping levels vary from about $\zeta = 0.020$ at $R = 1.2 \times 10^6$ to $\zeta = 0.032$ at $R = 4.8 \times 10^6$. Further discussion of these measurements is judged inappropriate.

3.1.5 Tests at constant kinetic pressure and velocity. With a cryogenic wind tunnel it is possible to select a combination of Mach numbers, total pressures and total temperatures such that both the kinetic pressure ($1/2\rho V^2$) and the velocity (V) remain constant[8]. It follows that the product, ρV, remains constant, so that for a particular model the aerodynamic damping and the frequency parameter will remain constant in the absence of Mach number effects. This is an interesting mode of testing for slender wings, where Mach number effects are small, at least for attached flows. For slender wings with separated flows, the angle of incidence for the formation of the tightly rolled vortices is also independent of Mach number, as Fig. 7 shows (based on Fig. 9a of Ref. 4). We have noticed already the large changes in the severity of buffeting on a slender wing after vortex breakdown, associated with changes in frequency parameter, so that a mode of testing at constant frequency parameter has many intrinsic advantages.

Fig. 8 illustrates such measurements on the three delta wings at Mach numbers of $M = 0.21$ and 0.35, where the Reynolds numbers are 1.9×10^6 and 4.8×10^6 respectively. For the aluminium wing (Fig. 8a) the steady bending-moment coefficients are much the same from $\alpha = 0°$ to 12°. However between $\alpha = 14°$ and 30° the $\overline{C}_B$ values at $M = 0.35$ are generally higher than at $M = 0.21$ due to the combined effects of the increase in Reynolds number and Mach number. It should be noted that the differences between the present measurements are smaller than those presented in Ref. 4 (shown by the dotted curves in Fig. 8a). With regard to the unsteady measurements, vortex breakdown occurs at about $\alpha = 22°$ at $M = 0.21$ and at about $\alpha = 24°$ at $M = 0.35$. After vortex breakdown the unsteady bending-moment coefficients are much the same but somewhat lower than the original measurements of Ref. 4 (which were almost identical at the two different Mach numbers). For the present tests the total dampings were about $\zeta = 0.012$ at $M = 0.21$ and about $\zeta = 0.020$ at $M = 0.35$. If the aerodynamic damping were constant (due to the constancy of ρV), this increase in total damping must be attributed to an increase in structural damping at the lower total temperature.

For the thick carbon fibre delta (Fig. 8b) the steady bending-moment coefficients have the same character but differ significantly, the slope $d\overline{C}_B/d\alpha$ generally being lower at $M = 0.21$ than at $M = 0.35$. In marked contrast, the unsteady bending-moment coefficients are virtually identical, with vortex breakdown occurring at about $\alpha = 22°$. It is significant that this excellent correlation of the unsteady measurements occurs when the total damping coefficients are almost identical. For this model ζ is about 0.016 at $M = 0.21$ and about 0.012 at $M = 0.35$, presumably due to a small decrease in structural damping at the lower total temperature if the aerodynamic damping is constant.

For the thin carbon fibre delta (Fig. 8c), the static bending-moment coefficients are identical from $\alpha = 0°$ to 22°, although the slope $d\overline{C}_B/d\alpha$ is lower than for the thick carbon fibre delta, and much lower than for the aluminium delta. Above $\alpha = 22°$ the static bending-moment coefficient is higher at $M = 0.21$ than at $M = 0.35$, a result which is inconsistent with the measurements on the other models and which appears anomalous. However, regarded as a Reynolds number effect, the anomaly would at least be consistent with that observed on this wing at $M = 0.35$ (*cf* Fig. 6c). In marked contrast to these differences between the steady bending-moment coefficients for $\alpha \geq 22°$, the unsteady bending-moment coefficients, although small, are virtually identical. Vortex breakdown occurs at about $\alpha = 24°$. Again it is interesting to note that this excellent correlation of the unsteady measurements occurs when the total damping values are almost identical. For this model ζ is about 0.030 at $M = 0.21$ and about 0.033 at $M = 0.35$, the small increase in total damping being attributed to a small increase in structural damping at the lower total temperature, on the assumption that the aerodynamic damping remains constant.

3.2 Unswept wing

The reader should recall that the present tests were made with fixed transition at $M = 0.30$, to provide a comparison with the previous measurements[4] made with free transition over the much wider Mach number range (from $M = 0.30$ to 0.80).

3.2.1 General description of flow and buffeting characteristics. No test results are available to describe the main features of the separated flow on this wing at low speeds and

no flow visualization, or pressure plotting was possible within the present tests. However, previous experience on other aerofoils and wings allows a tentative assessment to be made (Fig. 9).

For an NPL 9510 aerofoil at low Reynolds numbers (Fig. 9a), probably a small laminar leading edge separation bubble would form at moderate angles of incidence. This would be followed almost immediately by turbulent reattachment upstream of the roughness band. This tiny bubble would create no significant buffet excitation, or influence the overall forces, because of its short length. Thus the first significant excitation would be provided by a trailing-edge separation. This would move upstream steadily as the angle of incidence increases until the leading edge bubble bursts. With the trailing-edge separation there would be a gentle stall and a slow, progressive increase in buffeting. In this low Reynolds number range, increasing Reynolds number would reduce the size of the leading edge bubble and hence reduce the boundary layer thickness downstream. This would delay flow separation and hence reduce (or even eliminate) the buffeting. This would be consistent with the increase in the angle of incidence for buffet onset observed on the model wing as the Reynolds number increases from $R = 0.8 \times 10^6$ to 3×10^6, with both fixed and free transition (Fig. 10).

For the aerofoil at high Reynolds numbers (Fig. 9b) the laminar separation bubble would burst and extend fairly rapidly downstream, where it would merge with the trailing-edge separation moving upstream. If this assessment is correct, the first significant excitation would be provided by the leading-edge separation. In this high Reynolds number range the main effect of increasing the Reynolds number is probably to thin the boundary layer in the leading-edge region, thus making the effective leading-edge radius somewhat smaller. Hence this would tend to provoke leading edge separation and the angle of incidence for buffet onset should decrease[10]. This would be consistent with the decrease in the angle of incidence for buffet onset observed on the model wing as the Reynolds number increases from $R = 5 \times 10^6$ to 18×10^6. It is interesting to note that in this region of Reynolds number the angle of incidence for buffet onset observed on the model wing is a little higher with fixed transition, indicative of a sensitive flow condition in the vicinity of the leading edge.

Inevitably the three-dimensional flow on a low aspect ratio half wing is more complex than on an aerofoil, but it should be similar in character. Fig. 9c sketches the general character of the surface flow pattern expected with a trailing-edge separation at low Reynolds number. [This sketch is based on observations on a half wing of aspect ratio 1.5 and a NACA 4415 section given elsewhere[11].] Fig. 9d shows the general character of the flow expected at higher Reynolds number, with a leading-edge separation followed by reattachment and then a further separation towards the trailing edge.

With the separations sketched in Figs. 9c and d, the spanwise variations in the bubble length would provide a wide range of excitation frequencies. This excitation when integrated in space and time with respect to the first wing bending mode, would be expected to give a flat spectrum for $\sqrt{nG(n)}$ as a function of n. During the previous tests on this wing the total damping measurements showed less variation with the product $\rho \times V$ than on the delta wing. This was attributed primarily to the higher level of structural damping on the unswept wing, together with reduced aerodynamic damping (*cf* Figs. 13 and 12 in Ref. 4). The total damping measurements on the unswept wing in the present tests are not yet available but if we assume that the total damping is constant, the values of C_B would be expected to be independent of frequency parameter because of the flat excitation spectra.

This is as observed in the tests, which will be described shortly. Hence the measurements confirm that the excitation on this wing is fairly flat and due to three-dimensional bubble type separations, as observed on most other wings of moderate sweep and aspect ratio[1,10].

3.2.2 Tests at two constant total temperatures. During these tests at two constant temperatures (Figs. 11 and 12) the Reynolds number and kinetic pressure increase monotonically with the total pressure, so that the effects of changes due to Reynolds number and aeroelastic distortion are combined.

For tests at ambient total temperature, $T_t = 300$ K (corresponding with a test in a conventional, variable density tunnel) the static bending moment coefficients, $\overline{C}_B$, are identical at the three Reynolds numbers up to $\alpha = 8°$ (Fig. 11a). This suggests that with attached flow on the wing, the combined effects of variations in Reynolds number and static aeroelastic distortion are negligible. It is interesting to note that for $\alpha < 8°$ the slope $d\overline{C}_B/d\alpha$ is only about 2% less than estimated from aerofoil tests with this section at a Reynolds number of about 3×10^6 (See Appendix A and Ref. 11). Above $\alpha = 8°$ there are wide variations with total pressure which are not monotonic with total pressure. We will see later that this is because there are significant effects of both static aeroelastic distortion (section 3.2.3) and Reynolds number (section 3.2.4). These additional considerations allow us to offer an explanation of the curves of Fig. 11a.

For $p_t = 1.2$ bar the effects of static aeroelastic distortion are small and there is a maximum in $\overline{C}_B$ at $\alpha = 16°$. For the intermediate pressure ($p_t = 2.4$ bar) the effects of static aeroelastic distortion are larger and reduce $\overline{C}_B$, despite a small favorable scale effect due to the increase in Reynolds number. The reduction in $\overline{C}_B$ is comparable with that observed on the delta wing (*cf* discussion of Fig. 5) and is attributed to a nose down twist of the wing outboard sections. For the highest pressure ($p_t = 4.8$ bar) the favorable scale effects (due to the reduction of separation) increase $\overline{C}_B$ greatly and this increase must offset any further reduction in $\overline{C}_B$ due to increased wing twist. These complex changes in $\overline{C}_B$ suggest that in a conventional wind tunnel, operating at ambient total temperature over a range of total pressure, it would be virtually impossible to discriminate between the effects due to variations in Reynolds number and those due to aeroelastic distortion after flow separation.

In contrast to the confusion of the steady measurements, the unsteady measurements (Figs. 11b–d with $n = 0.27$) show monotonic changes, the incidence for buffet onset being respectively 8°, 9° and 13° and $p_t = 1.2$, 2.4 and 4.8 bar. These measurements suggest also that for a fixed penetration beyond buffet onset the severity of buffeting is much the same. This would be consistent with relatively small changes in total damping, as suggested in section 3.2.1.

For tests at a reduced total temperature, $T_t = 110$ K, Fig. 12a shows that the static bending-moment coefficients are identical at the two total pressures up to $\alpha = 11°$, which suggests once again that on this wing the combined effects of variations in Reynolds number and static aeroelastic distortion are negligible. This is consistent with the observation that in this range the slope $d\overline{C}_B/d\alpha$ is much the same as at $T_t = 300$ K (Fig. 11a) and again about 2% less than estimated from aerofoil tests. Above $\alpha = 11°$ there are wide variations with total pressure. Here the effects of static aeroelastic distortion (which reduces $\overline{C}_B$) and the scale effects (which are adverse and also reduce $\overline{C}_B$) are additive, so that the maximum

value of $\overline{C}_B$ is much lower at the higher total pressure. The influence of these additive, adverse effects on the unsteady measurements (Fig. 12b with $n = 0.46$) is to lower the incidence for buffet onset from $\alpha = 13°$ at $p_t = 1.2$ bar to $\alpha = 12°$ at $p_t = 4.8$ bar. These C_B measurements also suggest that for a fixed penetration beyond buffet onset the severity of buffeting is much the same. This would be consistent with the relatively small changes in total damping suggested in section 3.2.1.

3.2.3 Tests at constant Reynolds number and Mach number. Fig. 13 shows measurements for a constant Reynolds number of 3.1×10^6 obtained from two different combinations of total pressure, giving widely different values of kinetic pressure. With regard to the steady bending-moment coefficient, $\overline{C}_B$, there is a displacement equivalent to about 2° in the angle of incidence over the range from $\alpha = 0°$ to 11° (Fig. 13a). It seems best tentatively to attribute this displacement to zero errors in the measurement of $\overline{C}_B$ because the incidence for buffet onset (taken from the dynamic measurements) is $\alpha = 13°$ at both conditions (Fig. 13b). Above $\alpha = 13°$ the $\overline{C}_B$ values are reduced even further at the higher kinetic pressure (Fig. 13a), consistent with the trend observed in section 3.2.2. It is remarkable that for a fixed penetration beyond buffet onset at $\alpha = 13°$, the unsteady C_B values are much the same at both total pressures, despite the changes in frequency parameter, total damping and aeroelastic distortion (Fig. 13b).

3.2.4 Tests at constant kinetic pressure and Mach number. The large influence of Reynolds number at low speeds on this wing was illustrated by two tests with constant values of kinetic pressure. For the tests at low kinetic pressure (Fig. 14), the total pressure was 1.2 bar and the total temperature was reduced from 300 K to 110 K to increase the Reynolds number from 0.8×10^6 to 3.1×10^6. With regard to the steady bending-moment coefficients there are two effects (Fig. 14a). The first is a displacement in the incidence range from $\alpha = 0°$ to 8° which is again tentatively attributed to zero errors (as in the discussion of Fig. 13a). However above $\alpha = 0°$ much larger values of $\overline{C}_B$ are found at the higher Reynolds number, indicative of a strong favorable scale effect which inhibits the development of separations. This is consistent with the displacement of the angle of incidence for buffet onset from $\alpha = 8°$ to 13°, shown in the unsteady measurements (Fig. 14b). Once again, for a fixed penetration beyond buffet onset the severity of the buffeting is much the same.

For the tests at the high kinetic pressure (Fig. 15), the total pressure of 4.8 bar with three values of total temperature (300 K, 150 K and 110 K), gives Reynolds numbers of 3.1×10^6, 7.9×10^6 and 12.5×10^6. With regard to the steady bending-moment coefficients (Fig. 15a) the displacements of the curves over the incidence range from $\alpha = 0°$ to 12°, are consistent with zero errors. However above $\alpha = 12°$ there were large changes which were not monotonic with Reynolds number and which must represent serious and complicated scale effects. Thus the highest value of $\overline{C}_B$ (at $\alpha = 18°$) is 0.74 at $R = 3.1 \times 10^6$ (*cf* 0.84 at the same Reynolds number but a lower kinetic pressure in Fig. 14a), then $\overline{C}_B = 0.76$ at $R = 7.9 \times 10^6$ but falls to $\overline{C}_B = 0.67$ at $R = 12.5 \times 10^6$. Corresponding with these changes in the steady bending moment coefficients, for the unsteady measurements there is a systematic variation in the angle of incidence for buffet onset. This is $\alpha = 13°$ at $R = 3.1 \times 10^6$, increases to $\alpha = 14°$ at $R = 7.9 \times 10^6$ and falls to $\alpha = 12°$ at $R = 12.5 \times 10^6$. It is interesting to observe that at $\alpha = 18°$ there are also comparatively large variations in the unsteady values

of C_B associated with the variations in the study values of $\overline{C}_B$ discussed above. Despite the difficulties in making unsteady measurements with large separations, these differences in C_B are probably genuine and a further indication of scale effect at this high angle of incidence.

3.2.5 Influence of Mach number. The present tests were restricted to $M = 0.30$ but for completeness brief reference is made to the previous tests, which covered a much wider range of Mach number ($M = 0.18$ to 0.80). The main difficulty with those measurements is resolving the disparate effects due to variations in Mach number, Reynolds number and static aeroelastic distortion. The most helpful results (Ref. 4, Fig. 10m) are reproduced here as Fig. 16, which shows measurements at $M = 0.3$, 0.6, 0.7 and 0.8 with free transition. For $M = 0.6$, 0.7 and 0.8 the Reynolds numbers and kinetic pressures are not too different and hence Mach number effects should predominate over any effects due to aeroelastic distortion or Reynolds number.

The steady bending-moment coefficients (Fig. 16a) show much the same character from $M = 0.3$ to 0.7, the slopes in the attached flow region increasing steadily with Mach number. Beyond buffet onset, $\overline{C}_B$ continues to increase steadily with α. There is a radical difference in character at $M = 0.80$, with a well defined maximum in $\overline{C}_B$ at 9° (well above buffet onset at 8°) followed by a minimum at $\alpha = 11°$ (where the buffeting has a maximum). The unsteady bending-moment coefficients (Fig. 16b) are much the same in character from $M = 0.3$ to 0.7, the angle of incidence for buffet onset falling progressively as observed on many other wings[10]. Above buffet onset buffeting increases relatively slowly. However, for $M = 0.8$ there is a radical change in character, which matches that in the steady measurements. Buffet onset is sharply defined at $\alpha = 8°$ due to the rapid increase in buffeting.

Careful examination of the base levels of the C_B measurements shows that they are virtually constant over the incidence range from $\alpha = 0°$ to 8°. This is an interesting observation because in the incidence range from $\alpha = 0°$ to 4° we might expect trailing-edge separation to occur (at least according to the aerofoil tests of Ref. 12, which were made at a Reynolds number of about 2.7×10^6). The absence of such a change in the unsteady response must indicate one of three possibilities. The first possibility is that trailing-edge separation may not occur at these higher Reynolds numbers. The second possibility is that it does occur, but does not alter the wing buffeting. This has been observed by Roos[13] during buffeting tests on a supercritical aerofoil at $M = 0.82$. Such an observation would be contrary to the association commonly believed to hold between trailing-edge pressure divergence (indicative of trailing-edge separation) and buffet onset. Here again surface flow visualization would have been of interest. The third possibility is that trailing-edge separation does occur, but only causes light buffeting which is masked by the tunnel noise.

4. Discussion

The measurements presented above are reviewed now in a wider context. Manifestly one achievement is the confirmation that in a cryogenic wind tunnel the disparate effects of static aeroelastic distortion and Reynolds number can be better isolated whereas in a conventional pressurized wind tunnel, operating at ambient total temperatures, these effects are inextricably mixed.

Thus for the slender delta wings the present tests define the magnitude of scale effects and the effects due to aeroelastic distortion at $M = 0.35$ on both buffet onset and the severity of buffeting, together with the large effects of a variation in frequency parameter. In addition an indication that the angle of incidence for vortex breakdown increases with increasing Mach number can be inferred from the previous tests[4,5] (*cf* Fig. 7). Similarly for the unswept wing the present tests define the magnitude of scale effects and effects due to aeroelastic distortion at $M = 0.30$ on both buffet onset and the severity of buffeting, together with the small effects of a variation in frequency parameter. An indication that the angle of incidence for buffet onset decreases with increasing Mach number can be inferred from the previous tests (Fig. 16), consistent with observations on other wings with widely varying sections and higher aspect ratios[10].

When the results are examined closely some additional features are apparent. The first feature is that on both types of wing the largest scale effects are in the region of buffet onset, consistent with a general conclusion from a review of scale effects in unsteady aerodynamics[14]. The second feature relates to the choice of material for dynamic models in cryogenic wind tunnels, which lies between aluminium, carbon fibre composite and steel (which was not represented in these tests).

The carbon fibre material withstood the testing at low temperatures and had adequate structural damping. However, although the thick carbon fibre model provided a higher bending frequency than the aluminium wing, it was not as high as expected. This outcome (for the type of excitation spectrum typical of vortex breakdown shown in Fig. 3d), may be associated with increased static aeroelastic distortion compared to the aluminium wing. Tentatively this distortion has been attributed to twist near the wing tip, which could be due to reduced torsional stiffness caused by the lack of isotropy in the carbon fibre composite material. This hypothesis is consistent with the static torsional stiffness inferred from the wing torsional frequencies (Table 1). It is not clear whether this is peculiar to the method of fabricating these particular carbon fibre models. In future applications it is possible that carbon fibre models will only be used in cryogenic wind tunnels where high frequency parameters are essential (*eg* when models are being driven, as in the measurements of oscillatory pressure described previously[6,7]) and when such tests are restricted to low lift coefficients.

By the same reasoning, for general model testing steel alloys would be preferred to aluminium alloy because the static aeroelastic distortion will be smaller by a factor of 3, deriving from the ratio of Young's Modulus, E, for steel to that of aluminium. Identical models made in steel, aluminium and magnesium have the same frequencies for all modes because:

$$f \alpha \sqrt{\frac{E}{\rho_m}}, \tag{5}$$

and the ratio E/ρ_m is the same for these metals. A steel wing will, of course, give reduced aerodynamic damping, considered as a ratio to critical damping compared to an aluminium wing but this property (normally regarded as a disadvantage for buffeting tests*) is offset partially by the increase in aerodynamic damping for constant p_t associated with cryogenic temperatures[8,15].

*In contrast, for single degree of freedom flutter the reduced magnitude of the negative aerodynamic damping of the steel wing would normally be regarded as an advantage, because this would reduce the amplitude of the limit cycle oscillation encountered.

If steel or aluminium is the material selected for models in cryogenic tunnels the frequency may be too low on a solid model. This would be particularly serious for slender configurations (*cf* the excitation spectrum of Fig. 3d). However the frequency might be increased by locally lightening the model without reducing the stiffness, *eg* by hollowing out the centre of the wing. On the other hand, if the frequency of a steel or an aluminium model were too high, it could be lowered by the addition of heavy underwing stores (for a combat aircraft) or by the addition of engine nacelles (for a transport aircraft). This principle was discussed in Ref. 8.

It should be noted that even when made in steel, high aspect ratio model wings will suffer significant static aeroelastic distortion near the wing tip, although this will be less severe than a full-scale advanced transport aircraft with its flexible structure. Thus static aeroelastic distortion will be important at the tip where the local Reynolds numbers are low (particularly for winglets) and where accordingly scale effects are likely to be large. The tip region often makes an important contribution to the buffet excitation.

A number of limitations of these tests must be acknowledged. Perhaps the most serious limitation is the failure to derive the buffet excitation parameter, $\sqrt{nG(n)}$, from equation (3) for the aluminium wings, which had relatively small static aeroelastic distortion. However, this would have required measurements of the generalized mass (m) and dynamic calibration of the strain gauges (giving $\ddot{z}$). Some measurements of total damping, ζ, were derived from the spectra of the buffeting on the delta wings and these measurements are discussed briefly in Appendix B. There is no reason to doubt that if these calibrations had been made, the usual levels of buffet excitation parameter observed in wind tunnels[1,16], and in flight[1,3], would have been achieved.

Another limitation is the failure to measure the wind-on distortions of the wings and their overall forces. Without these measurements the observed anomalies in the $\overline{C}_B$ measurements cannot yet be explained (*cf* Appendix C). (Wind-on distortions have been measured successfully in a conventional wind tunnel using a photogrammetric technique[17] and it should be possible to use this in a cryogenic wind tunnel.)

Another limitation relates to the increased levels of tunnel noise at the highest frequency in the closed two-dimensional working section (Fig. 1b) used for the present tests. (This potential difficulty was recognized when the tests were suggested[18].) For all the delta wings the low level of buffeting associated with vortex formation (at about $\alpha = 5°$) is masked by the response due to the relatively high level of tunnel noise at that frequency. In the original tests[4] on the same aluminium delta wing (at about 490 Hz) in the other (slotted) two-dimensional working section, vortex formation also was observed clearly at about $\alpha = 5°$.

Fig. 17 compares some typical C_B measurements from the original NASA tests made in the top and bottom slotted working section (from Fig. 8d of Ref. 4) with previous RAE measurements[5] of $\sqrt{nG(n)}$ on the steel and magnesium models taken from Fig. 3c. [The scales for $\sqrt{nG(n)}$ and C_B have been selected to suggest that an affine transformation exists between the buffet excitation parameters and the buffeting coefficients. It may be seen by inspection of equations (2) and (3) that this would imply virtually constant damping for the C_B measurements.] For both series of tests vortex formation is marked clearly. For completeness, Fig. 17 includes the levels of $\sqrt{nG(n)}$ associated with light, moderate and heavy levels of buffeting according to well established criteria[1]. Vortex formation is

associated with very light levels of buffet at this frequency parameter, and hence can be masked easily by tunnel noise.

In contrast to the difficulty of determining vortex formation on the delta wings, throughout the present tests in the closed working section on the unswept wing (restricted to $M = 0.3$) there was no difficulty in determining buffet onset at $f = 270$ Hz (the lowest bending frequency within these tests). However, in the original tests buffet onset was not sharply defined at $M = 0.6$ and 0.7. This may have implied higher levels of tunnel noise in the two-dimensional slotted working section at those speeds, or possibly incipient trailing-edge separation.

Another limitation relates to the uncertainty about the types of flow separation on the unswept wing. When the tests were planned[8] it was recommended that surface flow visualization should always be made at buffet onset. However this recommendation could not be implemented for either the present or the original tests[4]. Although the authors believe that Figs. 9c and d give the correct general representation of the type of flow separation on the wing, they consider that an attempt should be made to compute the separation boundaries on an NPL 9510 aerofoil at $M = 0.30$. If predictions could be made over the Reynolds number range from 1×10^6 to say 20×10^6 this should suffice to confirm that the separations sketched in Figs. 9a and b do occur.

Despite these limitations, the tests show clearly that the dynamic buffeting technique works well in cryogenic facilities. Hence the authors recommend that it should be used (as a matter of routine) whenever flow separations are expected on models to be tested in cryogenic tunnels. This is particularly important when testing unorthodox configurations with unusual planforms (such as an X, W, Z or even diamond) because here the severity of buffeting, the magnitude of scale effects and the effects of aeroelastic distortion may be radically different from those on orthodox configurations.

Although half-models offer the advantage of the highest possible Reynolds number, they can only give the buffet excitation parameter in symmetric modes. Complete models have the disadvantage of providing lower Reynolds numbers (by a factor of $1/\sqrt{2}$ for the same blockage) but allow the buffet excitation parameter to be determined for both symmetric and anti-symmetric modes, as discussed in Ref. 1. In addition complete models are almost invariably supported on an internal, six-component strain gauge balance so that overall forces should be readily available to complement the buffeting measurements. However, for force balance measurements under buffeting conditions, special attention should be paid to the model dynamics on the sting so that balance fatigue failures do not occur. Criteria for structural damping levels in cryogenic wind tunnels are given in Ref. 19.

5. CONCLUSIONS AND RECOMMENDATIONS

This review suggests nine main conclusions and five recommendations with respect to buffeting tests in cryogenic wind tunnels. The conclusions are as follows:

(1) In a cryogenic wind tunnel the disparate effects of variations in Reynolds number and static aeroelastic distortion on wing buffeting can be better isolated, whereas in a conventional wind tunnel they are inextricably mixed.

(2) For delta wings above vortex breakdown the frequency parameter must be correctly represented because of the unusual type of excitation. In contrast, for the unswept wing the frequency parameter is relatively unimportant.

(3) Carbon fibre models can be tested successfully in cryogenic wind tunnels and the structural damping characteristics are satisfactory.

(4) Of all the materials (aluminium, carbon fibre and steel) considered for *routine* wing buffeting tests, steel is preferred because of the reduced static aeroelastic distortion at the wing tip.

(5) Carbon fibre may be used when very high frequency parameters must be achieved, *eg* for special tests when models must be oscillated without significant dynamic distortion. Careful lay-up of the fibres is required to ensure the requisite bending and torsional stiffness.

(6) For the delta wings tested, with sharp leading edges, scale effects are small up to the incidence for vortex breakdown, which itself does not vary strongly with Reynolds number for a constant Mach number.

(7) For the unswept wing scale effects are also small up to buffet onset.

(8) For the unswept wing buffet onset also varies strongly with Reynolds number in a way that suggests that there are two radically different types of incipient flow separation, depending upon the range of Reynolds number.

(9) For all the delta wings and the unswept wing the effects of static aeroelastic distortion are small below buffet onset but much larger above buffet onset. However, there are anomalous variations in $d\overline{C}_B/d\alpha$ for the delta wings which have not yet been explained (Appendix C).

The recommendations are as follows:

(a) Dynamic buffeting tests should be made as a matter of routine whenever wing models are tested in cryogenic wind tunnels. As in a conventional tunnel such buffeting measurements help to interpret the steady force measurements, to identify conditions suitable for flow visualization, and to identify incipient flow separations on the wing. Preferably these buffeting measurements should be expressed in terms of the buffet excitation parameter.

(b) For a given Mach number, these dynamic tests should always include some investigation of the effects of variations in Reynolds number, static aeroelastic distortion and frequency parameter, to allow precise extrapolation of the measurements to aircraft in flight.

(c) As in conventional tunnels, the levels of flow unsteadiness in cryogenic tunnels should be as low as possible and carefully measured. Tunnel operators should ensure that conditions (*eg* combinations of Mach number and fan speed) which produce high levels

of excitation at particular frequencies will not interfere with buffeting measurements on the model at the same frequencies.

(d) When testing unorthodox configurations with unusual planforms (such as an X, W, Z or even a diamond) the severity of buffeting, the magnitude of scale effects and the effects of aeroelastic distortion may be radically different from those on orthodox configurations. Hence these unorthodox configurations should be tested in cryogenic tunnels to predict the buffet excitation parameter, $\sqrt{nG(n)}$.

(e) Ideally static bending and torsion stiffnesses should be measured, perhaps in conjunction with the calibrations required to obtain $\overline{C}_B$ and $\sqrt{nG(n)}$. Ideally model static and dynamic deflections also should be measured during cryogenic tunnel tests.

Appendix A

ESTIMATION OF STEADY BENDING MOMENTS FOR BOTH WINGS AND COMPARISON WITH MEASUREMENTS

For the slender wings three well-known simple approximations [equations (A-1) to (A-3)] were used to estimate the static bending-moment coefficients and thus to identify the effect of the outboard displacement of the strain gauges from the root. Corresponding estimates for the unswept wing are more difficult, because the bending-moment slope must be inferred from the lift-curve slope measured on the same aerofoil. We shall show that these estimates are in excellent agreement with the measurements on the unswept wing.

Delta wings

According to slender wing theory the load distribution is elliptical and the centre of lift is given by:

$$\bar{y} = \frac{4}{3\pi} s. \tag{A-1}$$

However the leading-edge vortices would displace the centre of lift further outboard than suggested by equation (A-1). It is reasonable to assume that for the incidence range from $\alpha = 0°$ to $10°$ the normal force coefficient is almost the same as the lift coefficient so that:

$$C_N \simeq C_L = \left(\frac{\pi A}{2}\right) \alpha. \tag{A-2}$$

Hence from equations (1), (A-1) and (A-2):

$$\overline{C}_B = \left(\frac{\pi A}{2}\right) \frac{4\alpha}{3\pi} \frac{s}{\overline{\overline{c}}}. \tag{A-3}$$

Fig. 4a shows that equation (A-3) gives values much higher than the measurements.

This discrepancy is influenced by the displacement of the strain gauge centre from the model centre line. If the strain gauge centre is taken to be in the middle of the milled out area shown in Fig. 2a this displacement is about 0.94 cm or 0.1 s. The effect of this displacement is now estimated.

Suppose the elliptic loading is given by a local lift distribution:

$$C_L(y) = \frac{2A\alpha}{s^2} \sqrt{s^2 - y^2}. \tag{A-4}$$

Then the normal force outboard of the strain gauge is given by:

$$C_L = A\alpha \left[\theta + \frac{\sin 2\theta}{2}\right]_{\theta=\sin^{-1} 0.1}^{\theta=\frac{\pi}{2}} = \left(\frac{\pi A}{2}\right) \alpha(0.874), \tag{A-5}$$

rather than by equation (A-2).

In addition to the reduction in lift, the moment arm is reduced from (y) to $(y - 0.1\ \mathrm{s})$. Hence the moment coefficient is given by:

$$\begin{aligned}\overline{C}_B &= \left(\frac{\pi A}{2}\right)\frac{4\alpha}{\pi}\frac{s}{\overline{\overline{c}}}\left[-\frac{\cos^3\theta}{3} - 0.05\left(\theta + \frac{\sin 2\theta}{2}\right)\right]_{\theta=\sin^{-1}0.1}^{\theta=\frac{\pi}{2}} \\ &= \left(\frac{\pi A}{2}\right)\frac{4\alpha}{3\pi}\frac{s}{\overline{\overline{c}}}[0.779],\end{aligned} \tag{A-6}$$

rather than by equation (A-3).

Equation (A-6) is closer, but still more than twice as high as the measurements.

Unswept wing

A few steady measurements on an NPL 9510 aerofoil in a slotted wind tunnel are available at subsonic speeds over a narrow range of angle of incidence where the flow is fully attached. From Figs. 4 to 8 of Ref. 12, we find that at $M = 0.5$ and a Reynolds number of 2.7×10^6 (with transition at 6 to 8% chord on the lower surface and at 4 to 6% chord on the upper surface):

$$\frac{dC_L}{d\alpha} = 6.88/\text{radian}. \tag{A-7}$$

Then according to the Prandtl-Glauert law for aerofoils:

$$\sqrt{(1 - M^2)}\,\frac{dC_L}{d\alpha} = \text{Constant}. \tag{A-8}$$

The lift curve slope at $M = 0$ would be lower and given by:

$$\frac{dC_L}{d\alpha} = 6.88\sqrt{1 - (0.5)^2} = 5.96/\text{radian}. \tag{A-9}$$

If we assume that the interference in the slotted tunnel used for these aerofoil tests was small (as the authors of Ref. 11 suggested), equation (A-9) may be used to determine the factor k, which represents the loss of lift on an aerofoil due to the boundary layer thickness, according to the relation:

$$k = \frac{1}{2\pi}\frac{dC_L}{d\alpha} = \frac{5.96}{6.28} = 0.95. \tag{A-10}$$

These results for an aerofoil must now be applied to a wing of finite aspect ratio, A, at a Mach number M. For an elliptic wing with an elliptic loading the expression given by Glauert for $M = 0$ can be modified to:

$$\frac{dC_L}{d\alpha} = \frac{2\pi k}{\sqrt{1 - M^2}}\,\frac{1}{1 + \frac{2k}{A\sqrt{1-M^2}}}. \tag{A-11}$$

The present half model of aspect ratio 1.5 is equivalent to a complete wing of aspect ratio 3. Hence at $M = 0.3$, from equations (A-10) and (A-11) we find that:

$$\frac{dC_L}{d\alpha} = 3.76. \tag{A-12}$$

For an elliptic load distribution, the centre of lift acts as a spanwise distance from the centre line given by equation (A-1).

Hence from equations (A-12) and (1) the estimated value of the bending-moment coefficient slope becomes:

$$\frac{dC_B}{d\alpha} = \frac{dC_L}{d\alpha}\frac{\bar{y}}{\bar{\bar{c}}} = 3.76 \times (0.425) \times 1.5 = 2.40/\text{radian}. \tag{A-13}$$

The measured value for the model wing from Fig. 15a for $R = 3.1 \times 10^6$ is about:

$$\frac{dC_B}{d\alpha} = 2.37/\text{radian}. \tag{A-14}$$

Equations (A-13) and (A-14) must be regarded as being in excellent agreement, considering the large number of assumptions made in deriving the estimates and the difficulty of making the measurements accurately, particularly at cryogenic temperatures.

Appendix B

ESTIMATION OF THE AERODYNAMIC DAMPING FOR THE THREE DELTA WINGS AND COMPARISON WITH MEASUREMENTS

It is convenient to express estimates of aerodynamic damping in terms of the ratio to critical damping. For flat plate wings this introduces a dependence upon the model density and thickness. For slender wings of uniform thickness, t, three analytic solutions for the aerodynamic damping, γ, due to vibration in the first bending mode were derived in Appendix E of Ref. 5. The preferred expression, from quasi-steady slender wing theory in which the aerodynamic damping force on the bending wing is derived from the cyclic changes in effective incidence is:

$$\gamma = \left(\frac{\rho}{\rho_m}\right) \left(\frac{v}{t\omega}\right) S_T \frac{5\pi}{8}, \tag{B-1}$$

where m = model density,
$\omega = 2\pi f$ (radians/s),
S_T = ratio of semi-span/root chord (0.46 for a 65° delta).

This expression gave good agreement with the aerodynamic damping measured on both the steel and magnesium wings in Ref. 5. Hence good agreement would also be expected for the present tests. The numerical values needed in equation (B-1) are given in the following table.

Wing	$t\omega$ (m/s)	Density ρ_m (g/cm^3)
Aluminum	15.4	2.80
Thick carbon fibre	20.8	1.64
Thin carbon fibre	5.8	1.71

In all three wings the wind-off structural damping is at about the same level, namely:

$$g/2 = 0.005. \tag{B-2}$$

Since there is no evidence that the structural damping changes significantly due to variations in amplitude, normal force or total temperature, the total damping, ζ, becomes:

$$\zeta = \gamma + g/2 = \left(\frac{\rho}{\rho_m}\right) \left(\frac{v}{t\omega}\right) 0.903 + 0.005. \tag{B-3}$$

This theoretical, linear expression is plotted in Fig. 18 together with the measured values. The measurements have no clear systematic variation with the angle of incidence (as in the tests of Ref. 5) and are scattered about the theoretical expression. The scatter is much higher than in the tests of Ref. 5, where the 'random-decrement' method was used to determine the total damping. In the present tests the measurements may be more scattered due to variations in structural damping with amplitude, normal force or total temperature, or to a less accurate method of determining the damping, or to a combination of all these effects. Variations in structural damping are known to occur—(*cf* discussion of Fig. 8a).

Whatever the cause of the scatter, the aerodynamic damping (which represents the dynamic lift due to wing motion in the first bending mode) is adequately predicted by slender wing theory. Hence the steady lift should also be accurately described by slender wing theory as expressed by equation (4).

Appendix C

SOME UNEXPLAINED ANOMALIES

Two anomalies have appeared during these tests. The first is that the increase in torsional stiffness expected of the carbon fibre deltas was not achieved. The second is that the carbon fibre deltas generally give slopes $d\overline{C}_B/d\alpha$ lower than those observed on the aluminum delta. These anomalies may be related and the following comments are offered.

With regard to the loss of stiffness, a value of E in bending about 1.03 × that of aluminum was expected from the unidirectional carbon fibre tape used and the lay-up selected (0°, 45°, 90° and −45°). Table 1 shows that the bending stiffness inferred from the bending frequency and the measured densities for the thick carbon fibre was about the same as that for the aluminum wing. This is consistent both with the expected bending stiffness and with the values of Young's Modulus inferred from the static deflections due to load, which were almost identical on the aluminum and thick composite delta wings. However the torsional modulus inferred from the torsional frequency was less for the thick carbon fibre delta than for the aluminum delta (0.76 instead of 1, Table 1). This reduction in torsional rigidity would be consistent with larger wing twists at the tip (due to static aeroelastic distortion) which would be expected to reduce the $\overline{C}_B$ values. No figure for torsional stiffness is quoted for the uni-directional tape.

With regard to the anomalous slopes, $d\overline{C}_B/d\alpha$, the major problem is in the incidence range from $\alpha = 0°$ to 8°. Here the measurements on the three wings generally show no variation with kinetic pressure, suggesting that the effects of static aeroelastic distortion are small. This is a reasonable result, because here the vortex is small and the buffeting low. There are two exceptions when individual wings suggest aeroelastic distortion: the thin wing in Fig. 5c in the range $10° \leq \alpha \leq 20°$ and for the thick wing in Fig. 8b in the range $0° \leq \alpha \leq 18°$.

In contrast to this result for the individual wings, the slope, $d\overline{C}_B/d\alpha$, varies from wing to wing in a systematic way, as the table shows (slopes taken from Fig. 5 and the prediction according to equation (A-6)).

Delta Wing	$d\overline{C}_B/d\alpha$
Aluminum	0.40
Thick CF	0.32
Thin CF	0.30
Predicted (A-6)	0.49

No corresponding changes in normal force curve slope were observed during the tests of the steel and magnesium deltas reported in Ref. 5. (Results from those tests are reproduced in Fig. 3a).

It is difficult to explain the variation in the present tests. Possibilities considered and rejected include:

(1) Some subtle model to model difference in the root fixing, which was nominally encastré. For the aluminum delta the root block was screwed directly into the aluminum turntable. Both carbon fibre wings were bonded to carbon fibre root blocks, tapered in the spanwise direction. These were then inserted into a matching taper provided in the aluminum turntable. All three end constraints are thought to have provided encastré conditions.

(2) Some influence of fluctuating bending moments on the measurements of the mean bending moment. This must be rejected because the buffeting levels are low in this incidence range. In addition a careful test calibration of the instrumentation described in sections 2.3 and 2.4 shows that fluctuating bending moments do not affect the mean bending moment. This assurance is valuable because of the large changes in C_B which occur after vortex breakdown ($\alpha > 22°$).

(3) Wrong calibration factors for the wings. This explanation must be rejected because the static calibration factors have been repeated. The major anomalies occur for the carbon fibre deltas and for these the change in calibration factor is only 2% from 300 K to 110 K (*cf* section 2.4).

The authors consider that these unexplained anomalies should not be allowed to detract from the main achievement: successful buffeting tests in a cryogenic wind tunnel over a very wide range of frequency parameter. These anomalies alter neither the conclusions nor the recommendations. However these anomalies re-iterate the importance of careful static and dynamic calibrations in buffeting tests, and the importance of obtaining good overall force data from balances during tests when the effects of variations in Reynolds number and static aeroelastic distortion are being evaluated.

Table 1

DETAILS OF DELTA WINGS

Delta wing	Thickness (mm)	First bending frequency (Hz)	Relative bending modulus (E) inferred from frequency and density	Relative bending modulus (E) inferred from deflection measurements	Wind-off structural damping at ambient conditions (fraction critical) (bending mode)	First torsion frequency (Hz)	Relative torsion modulus inferred from frequency and density	Relative static torsional stiffness
Thick carbon fibre	5.1	650	1.07	1.00	0.0050	1630	0.74	0.74
Aluminum	5.1	480	1.00	1.00	0.0033	1450	1.00	1.00
Thin carbon fibre	2.5	360	1.43	1.62	0.0057	1450	2.54	$2.54/(2.04)^3 = 0.30$

Inferred Young's Modulus for bending for the thick carbon fiber wing is about the same as that for aluminium, *ie*

$$E = 73 \text{ GN/m}^2 \ (10 \times 10^6 \text{ lb/in}^2).$$

Specification values for bending of Magnamite Graphite Pre-Preg tape AS4/3502 with unidirectional graphite fibres is higher than this:

$$E = 124 \text{ GN/m}^2 \ (18 \times 10^6 \text{ lb/in}^2).$$

Fibre lay-up orientations are (0°, 45°, 90°, −45°, 0°) which are consistent with the unidirectional values.

LIST OF SYMBOLS

A	aspect ratio of complete wing
$\overline{C}_B$	static bending-moment coefficient (equation (1))
C_B	dynamic bending-moment coefficient (equation (2))
C_L, C_D, C_m	lift, drag and pitching moment coefficients
C_N	normal force coefficient
c	local chord
$\overline{\overline{c}}$	aerodynamic mean chord of wings
E	Young's Modulus
f	frequency (Hz) in bending mode
k	factor representing loss of lift on aerofoil due to boundary layer (equation (A-10))
$g/2$	structural damping coefficient (fraction critical) (equation (B-2))
M	Mach number
m	generalized mass
$\sqrt{nG(n)}$	buffet excitation parameter (equation (3))
$n = f\overline{\overline{c}}/V$	frequency parameter
p_t	total pressure
$q = 1/2\rho V^2$	free stream kinetic pressure
R	Reynolds number based on $\overline{\overline{c}}$
S	wing area
S_T	ratio of wing semi-span/root chord (equation (B-1))
s	wing semi-span from centre line
T_t	total temperature
t	wing thickness
x	streamwise co-ordinate
y	spanwise co-ordinate

$\bar{y}$	distance from centre line of spanwise centre of lift
$\ddot{z}$	rms tip acceleration in mode
V	free stream velocity
α	wing and incidence
γ	aerodynamic damping coefficient fraction of critical (equation (B-1))
ζ	total damping, fraction of critical (equation (3))
ρ	free stream density
ρ_m	model density
$\omega = 2\pi f$	circular frequency (radians/s)

References

1. Mabey, D. G.: Some aspects of aircraft dynamic loads due to flow separation. *Prog. Aerospace Sci. 26,* pp. 115–151 (1989) or AGARD R750 (1988).

2. Huston, W. B.: *A study of the correlation between flight and wind tunnel buffet loads.* AGARD Report 121 (1957).

3. Jones, J. G.: *A survey of the dynamic analysis of buffeting and related phenomena.* RAE Technical Report 72197 (1972).

4. Boyden, R. P.; and Johnson, W. G., Jr.: *Results of buffeting tests in a cryogenic wind tunnel.* NASA TM 84520 (1982).

5. Mabey, D. G.; and Butler, G. F.: *Measurements of buffeting on two 65° delta wings of different materials.* RAE Technical Report 76009 (1976).

6. Mabey, D. G.; and Welsh, B. L.: Measurements and calculations of steady and oscillatory pressures on a low aspect ratio model at subsonic and transonic speeds. *J. Fluids and Structures,* I, pp. 445–468 (1987).

7. Mabey, D. G.; Welsh, B. L.; and Pyne, C. R.: A summary of measurements of steady and oscillatory pressures on a rectangular wing. *Aero J. R Aero Soc.* (1988).

8. Mabey, D. G.: *Some remarks on dynamic aeroelastic model tests in cryogenic wind tunnels.* NASA CR-145029 (1975).

9. Cole, H. A., Jr.: *On-the-line analysis of random vibrations.* AIAA Paper No. 68-288 (1968).

10. Mabey, D. G.: Buffeting criteria for a systematic series of wings. *AIAA J. Aircraft, 26,* part 6, pp. 576–582 (1989).

11. Bippes, H.; Jakob, K.; and Turk, M.: *Experimental investigations of the separated flow around a rectangular wing in a wind tunnel.* DFVLR-FB-81-12 (1981).

12. Hall, D. J.; Quincey, V. G.; and Lock, R. C.: *Some results of wind-tunnel tests on an aerofoil section (NPL 9510) combining a 'peaky' upper surface pressure distribution with rear loading.* ARC CP 1292 (1974).

13. Roos, F. W.: Some features of the unsteady pressure field in transonic aerofoil buffeting. *AIAA J. Aircraft, 17,* Part 11, 781–788 (1980).

14. Mabey, D. G.: *A review of scale effects in unsteady aerodynamics.* RAE Technical Report 91007 (1991), to be published in Prog. Aerospace Sci.

15. Mabey, D. G.; Ashill, P. R.; and Welsh, B. L.: Aeroelastic oscillations caused by transitional boundary layers and their attenuation. *AIAA J. Aircraft, 24,* Part 7, pp. 463–469 (1987).

16. Zan, S. J.; and Maull, D. J.: *The effect of wing planform on low-speed buffet.* AGARD CP 483, Paper 12 (1990).

17. Byrdsong, T. A.; Adams, R. R.; and Sandford, M. C.: *Close-range photogrammetric measurement of static deflections for an aero-elastic supercritical wing.* NASA TM 4194 (1990).

18. Mabey, D. G.: *Some remarks on the design of transonic tunnels with low levels of flow unsteadiness.* NASA CR 2722 (1976).

19. Mabey, D. G.; Welsh, B. L.; and Pyne, C. R.: *The reduction of rigid-body response of sting supported models at high angles of incidence.* RAE TR 89012 (1989).

    Also *"A review of rigid-body response of sting supported models at high angles of incidence"* to be published in Prog. Aerospace Sci., Vol. 28, pp. 133–170, 1991.

20. Glauert, H.: *Elements of aerofoil theory.* Published Cambridge University Press Chapter XI, p. 145 (1948).

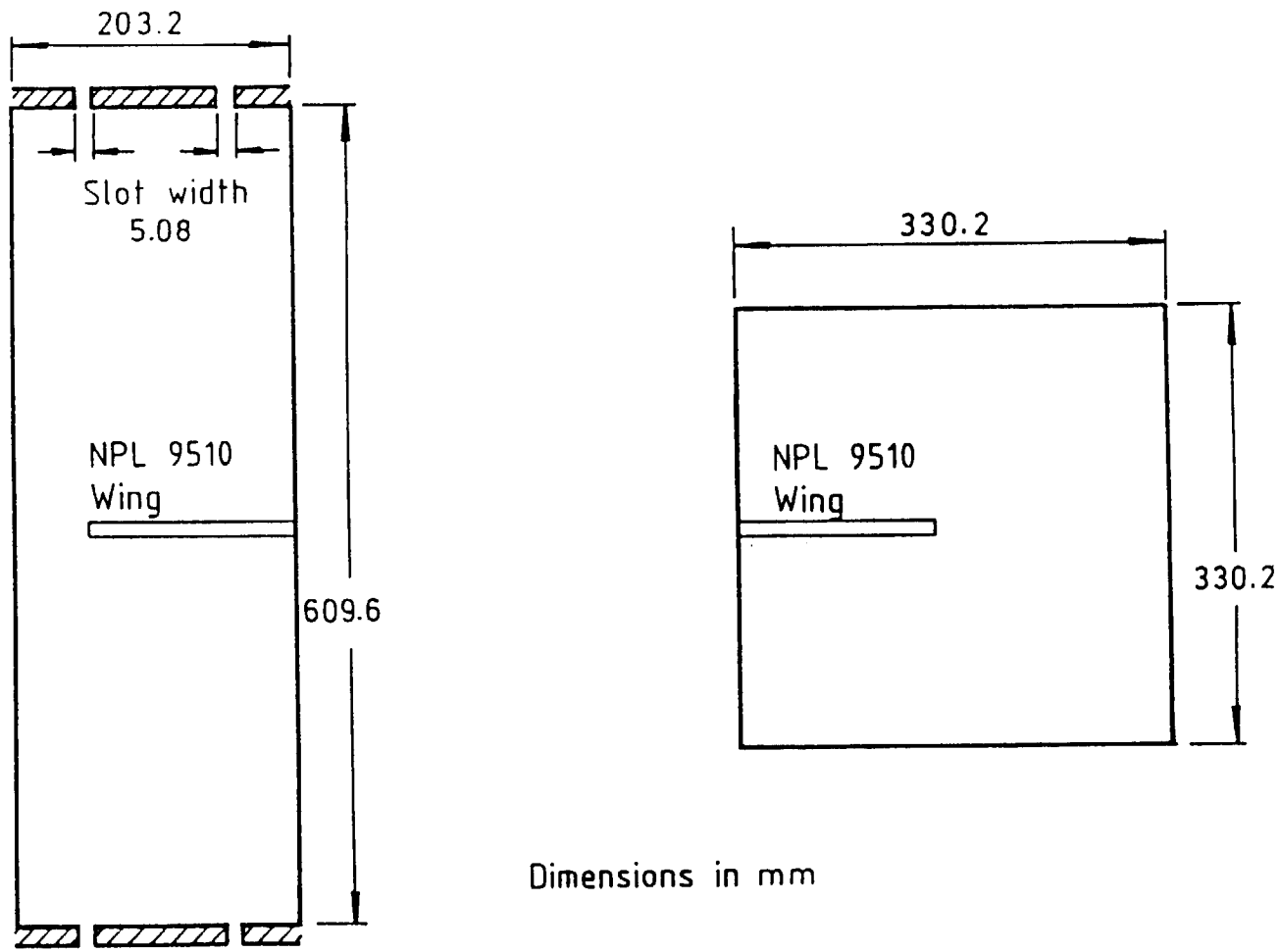

a) Two-dimensional top and bottom slotted test section

b) Two-dimensional closed adaptive wall test section

Fig 1 Test sections of the 0.3 Meter Transonic Cryogenic Tunnel

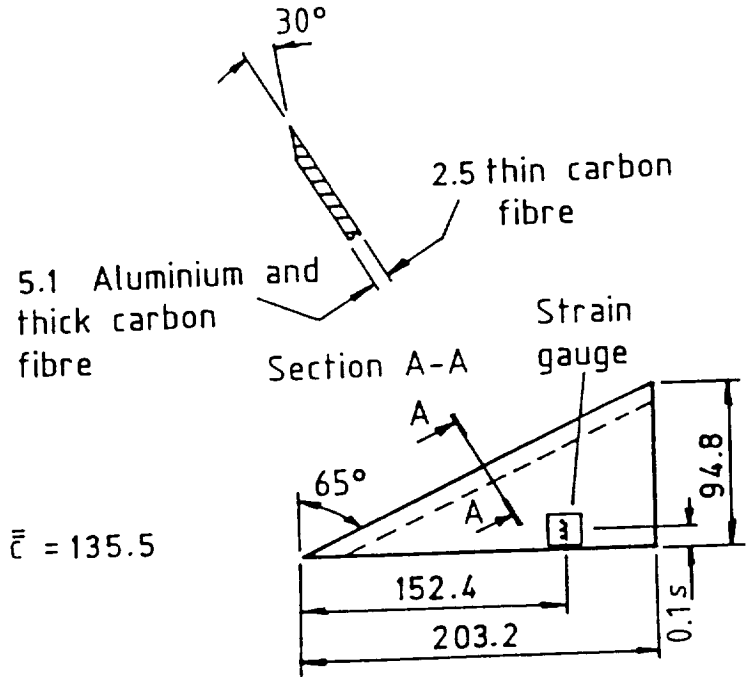

a) Delta wings

Dimensions in mm

After Ref. 4

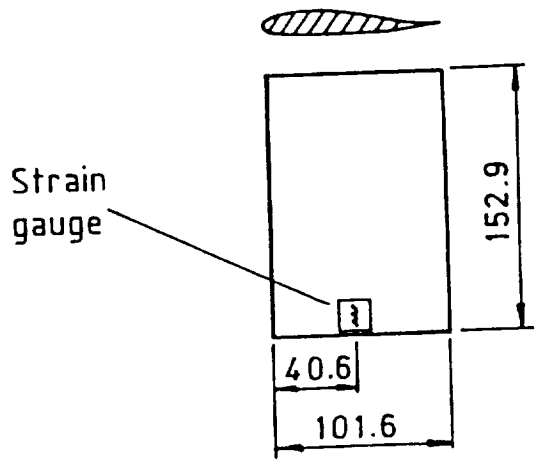

b) Unswept NPL 9510 wing

Fig 2 Models used for buffeting tests

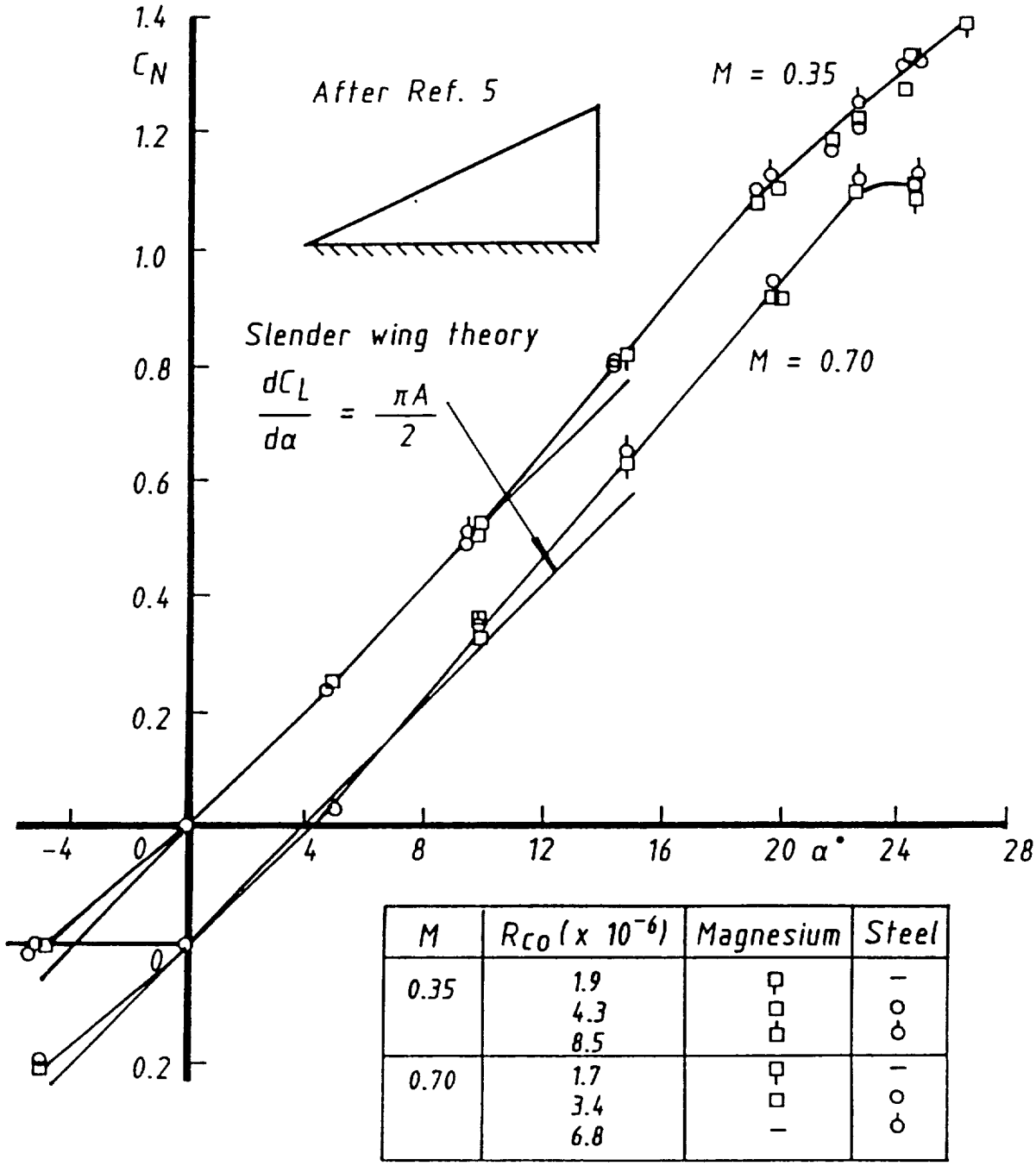

M	R_{co} (x 10^{-6})	Magnesium	Steel
0.35	1.9	⊡	—
	4.3	□	○
	8.5	⊡	○
0.70	1.7	⊡	—
	3.4	□	○
	6.8	—	○

a) Variation of normal force coefficient with angle of incidence

Fig 3 Main features of forces and flows on delta wings

Fig 3 continued

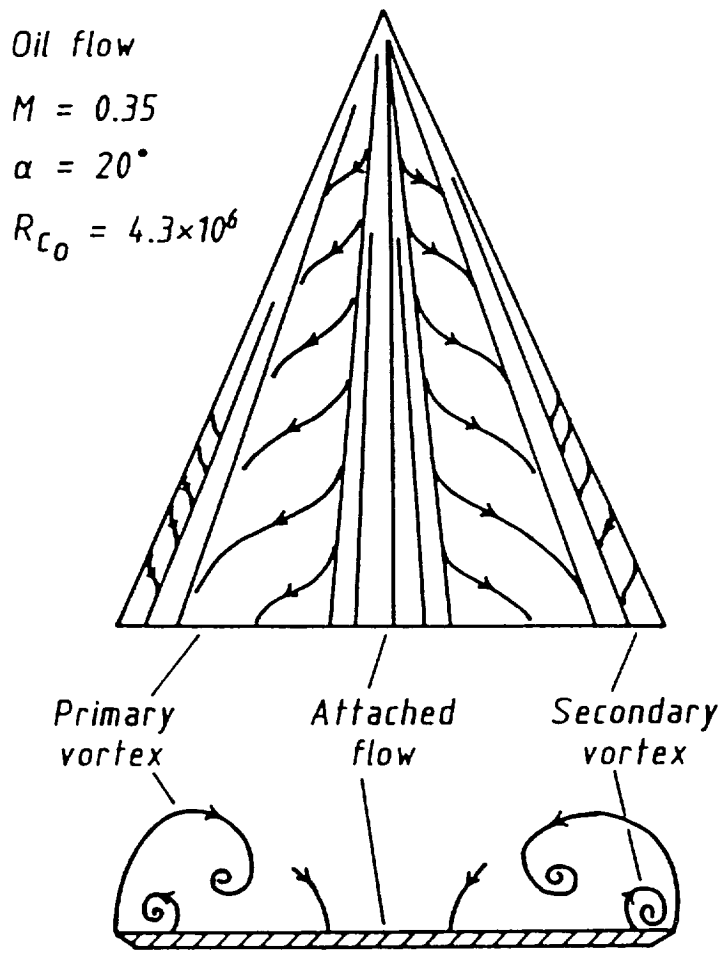

(b) Flow separations

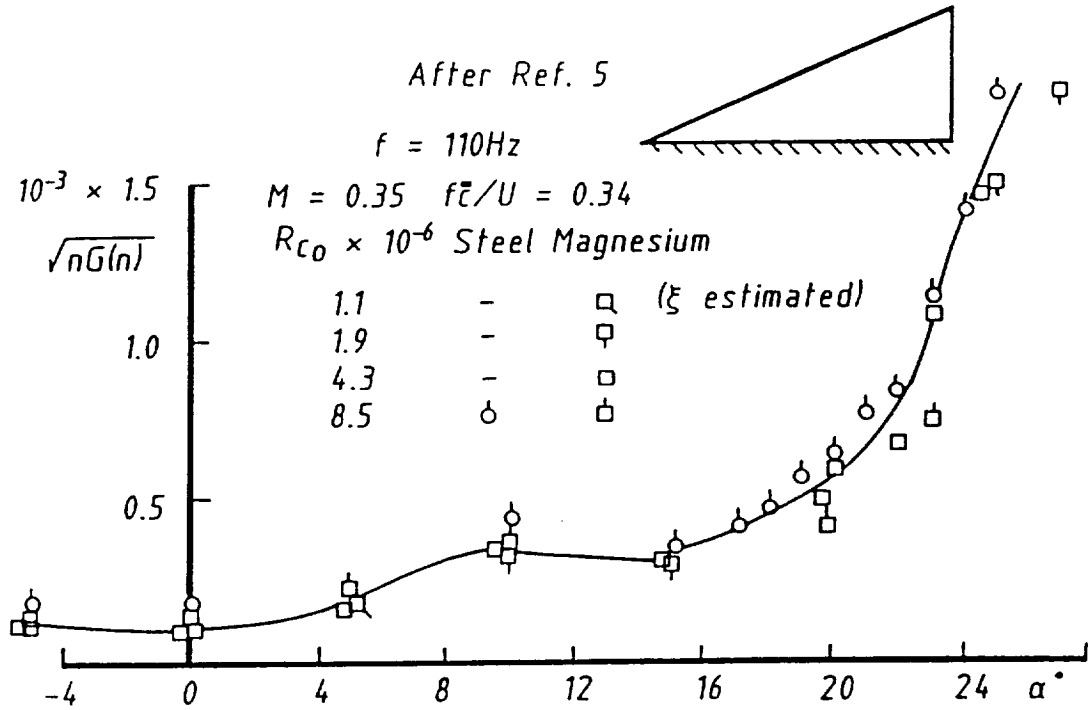

c) Variation of buffet excitation parameter with angle of incidence

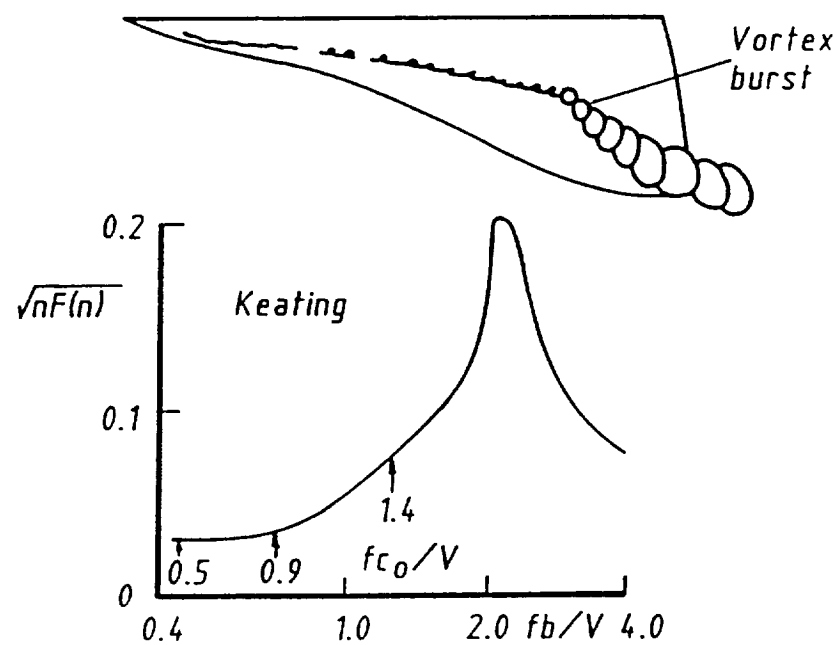

d) Spectrum with vortex breakdown

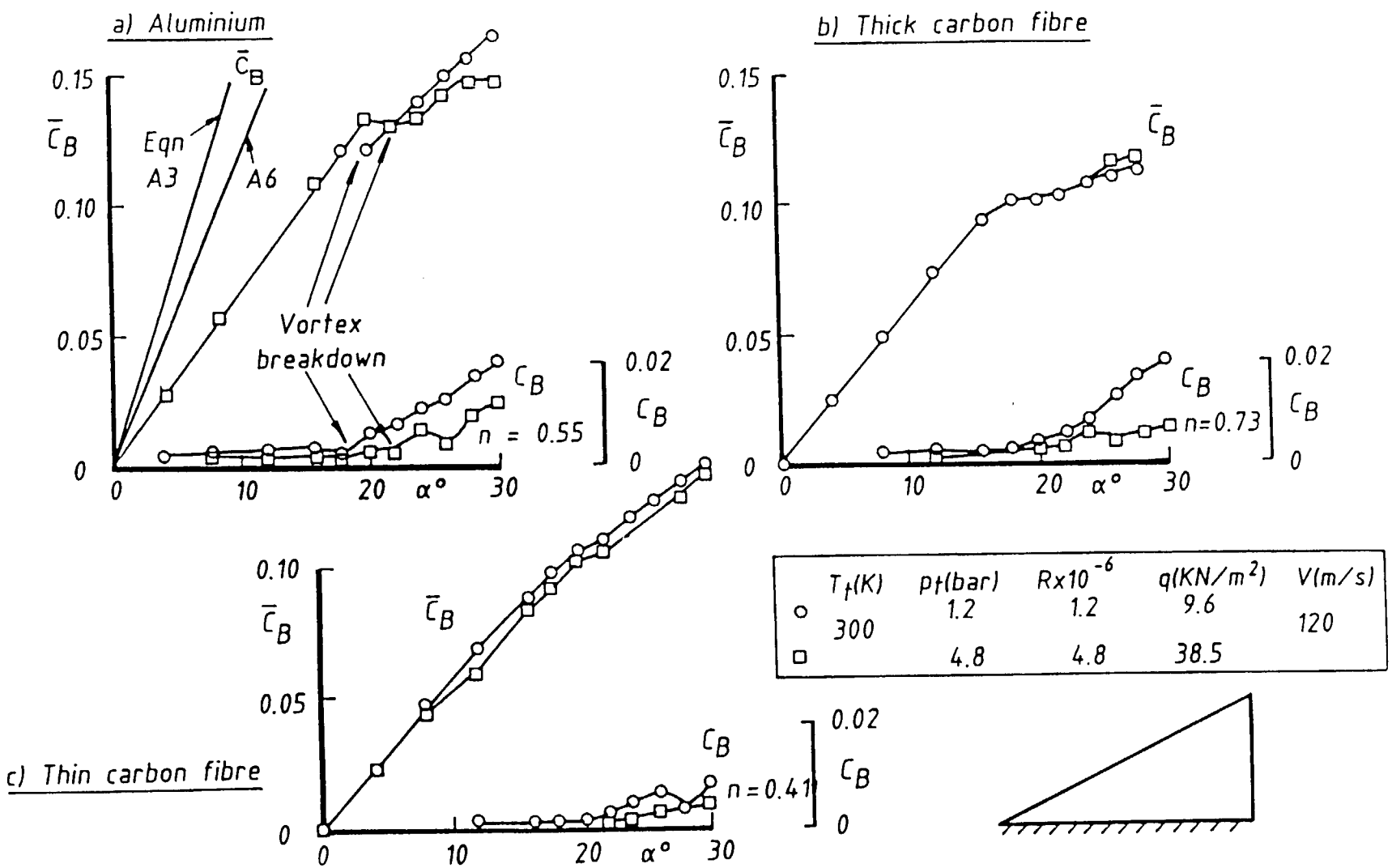

Fig 4 Tests at ambient total temperature on delta wing (M = 0.35)

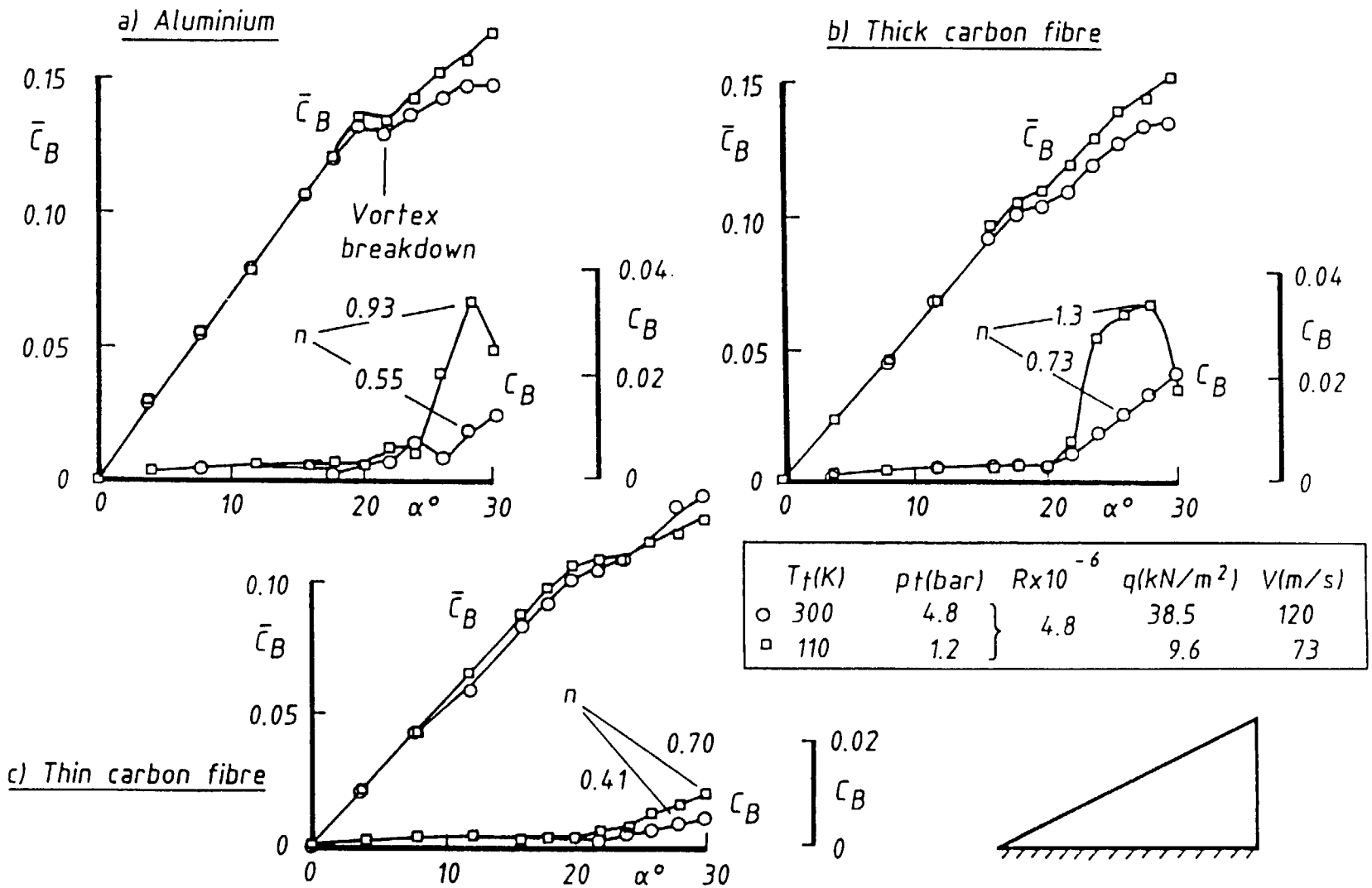

Fig 5 Tests at constant Reynolds number and Mach number (M = 0.35)

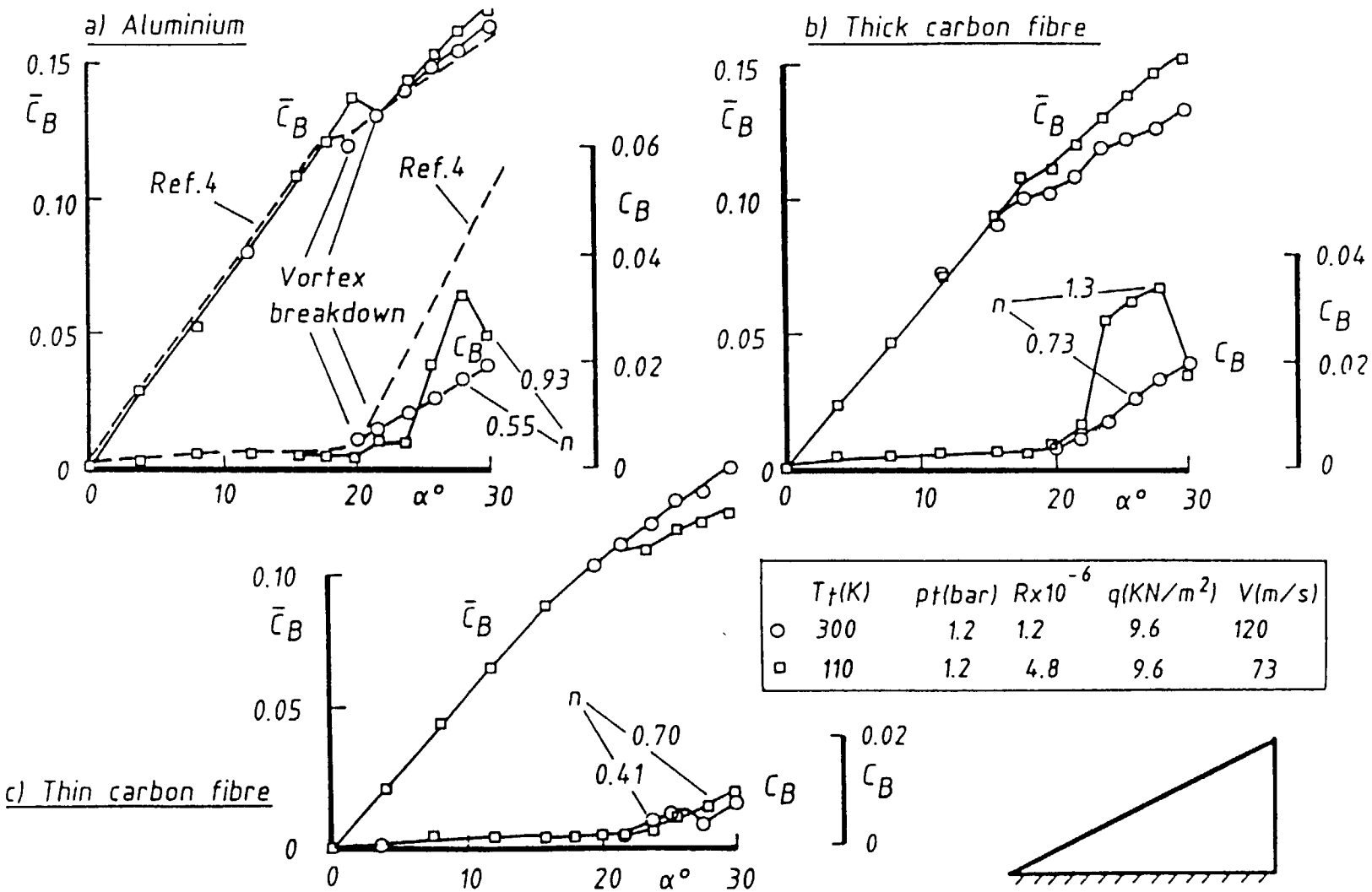

Fig 6 Tests at constant kinetic pressure and Mach number (M = 0.35)

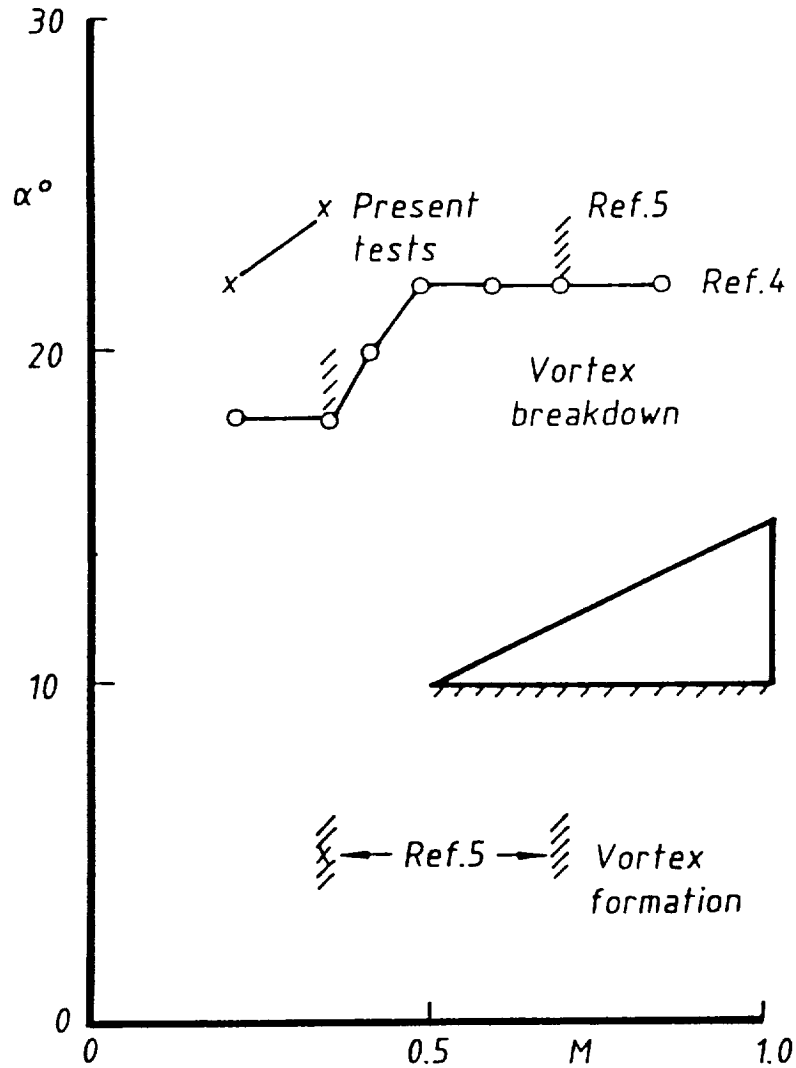

Fig 7 Mach number effect on vortex formation and vortex breakdown

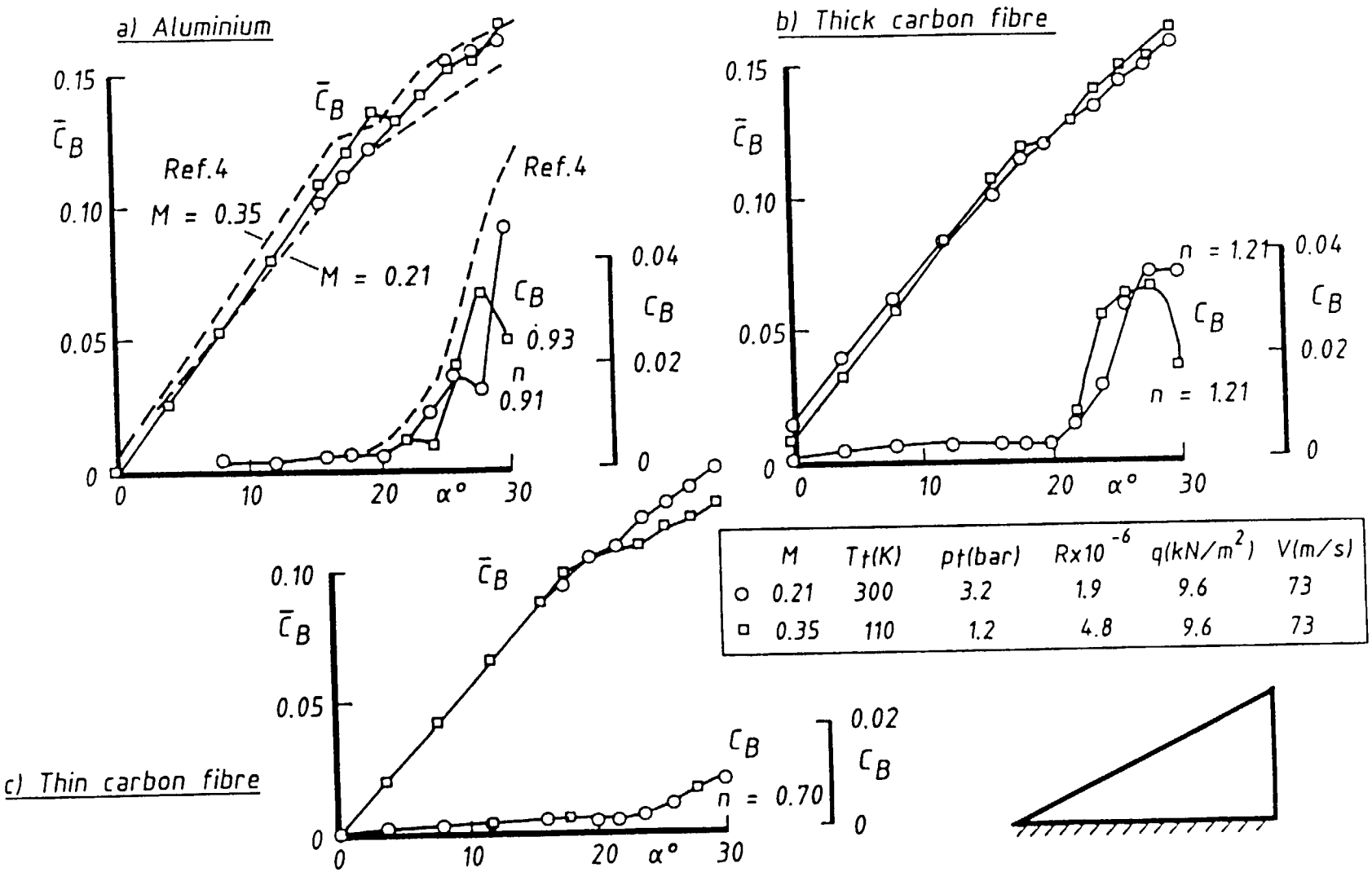

	M	Tt(K)	pt(bar)	$Rx10^{-6}$	$q(kN/m^2)$	V(m/s)
○	0.21	300	3.2	1.9	9.6	73
□	0.35	110	1.2	4.8	9.6	73

Fig 8 Tests at constant kinetic pressure and velocity

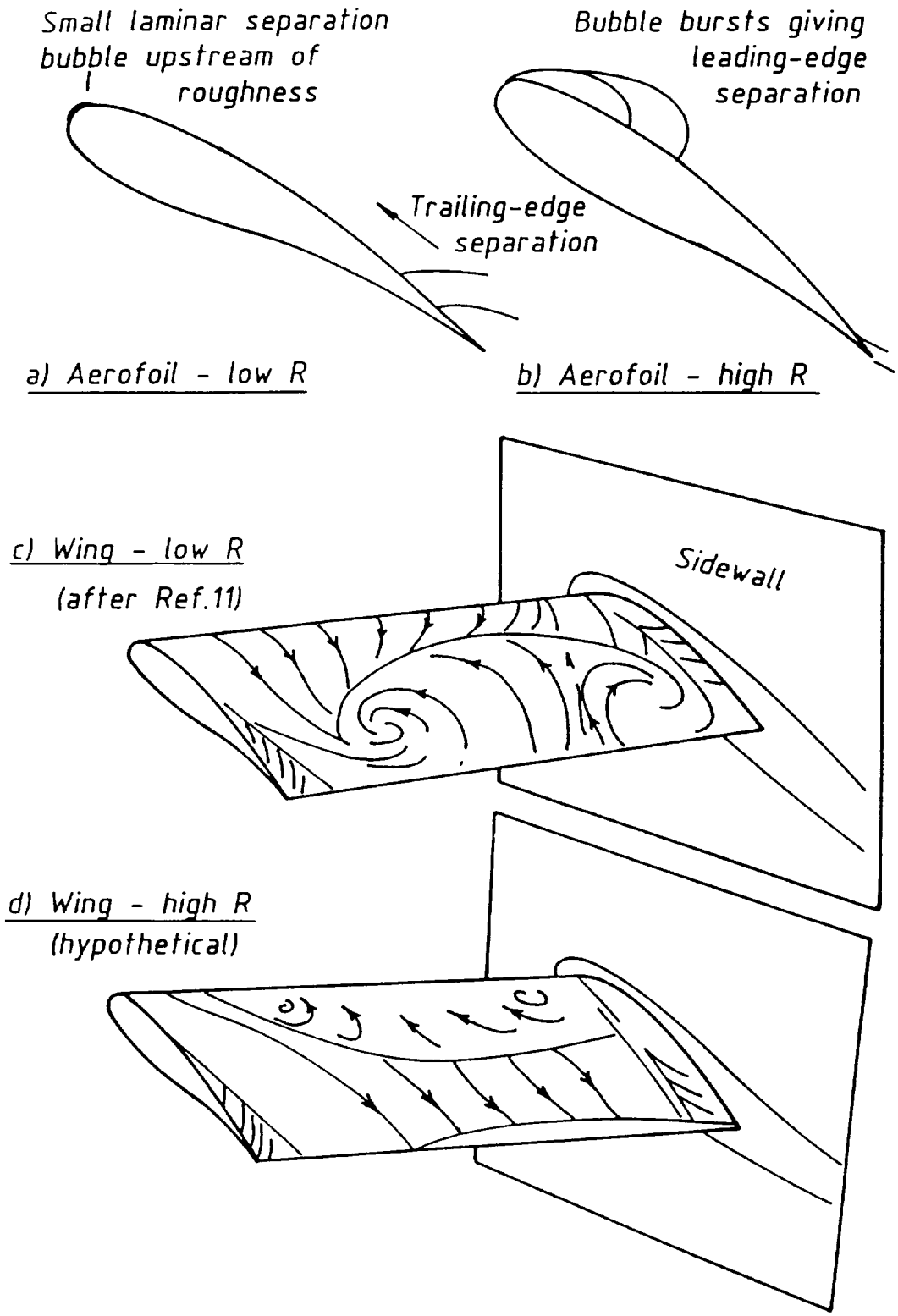

Fig 9 Tentative assessment of flows near buffet onset at low and high Reynolds numbers

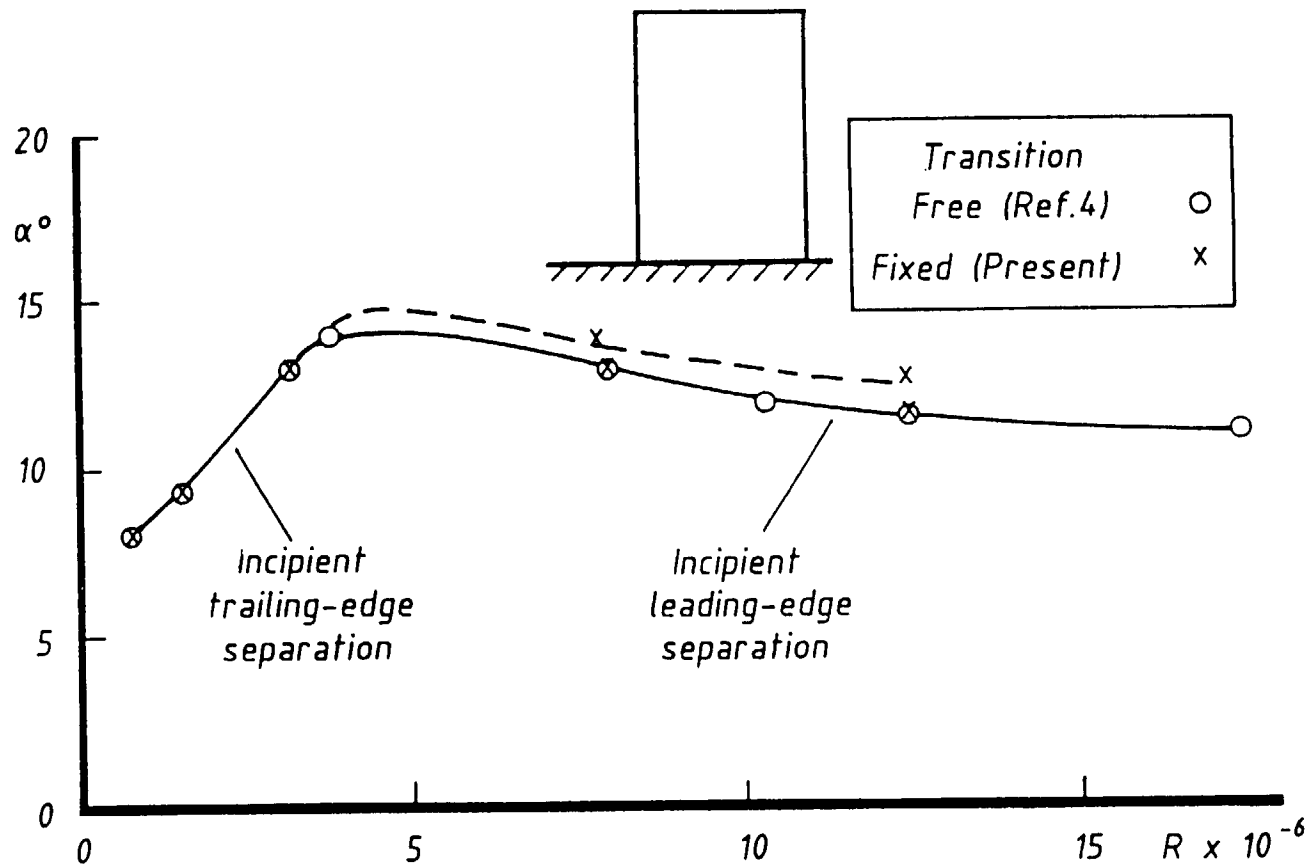

Fig 10 Effect of Reynolds number on angle of incidence for buffet onset for NPL 9510 wing

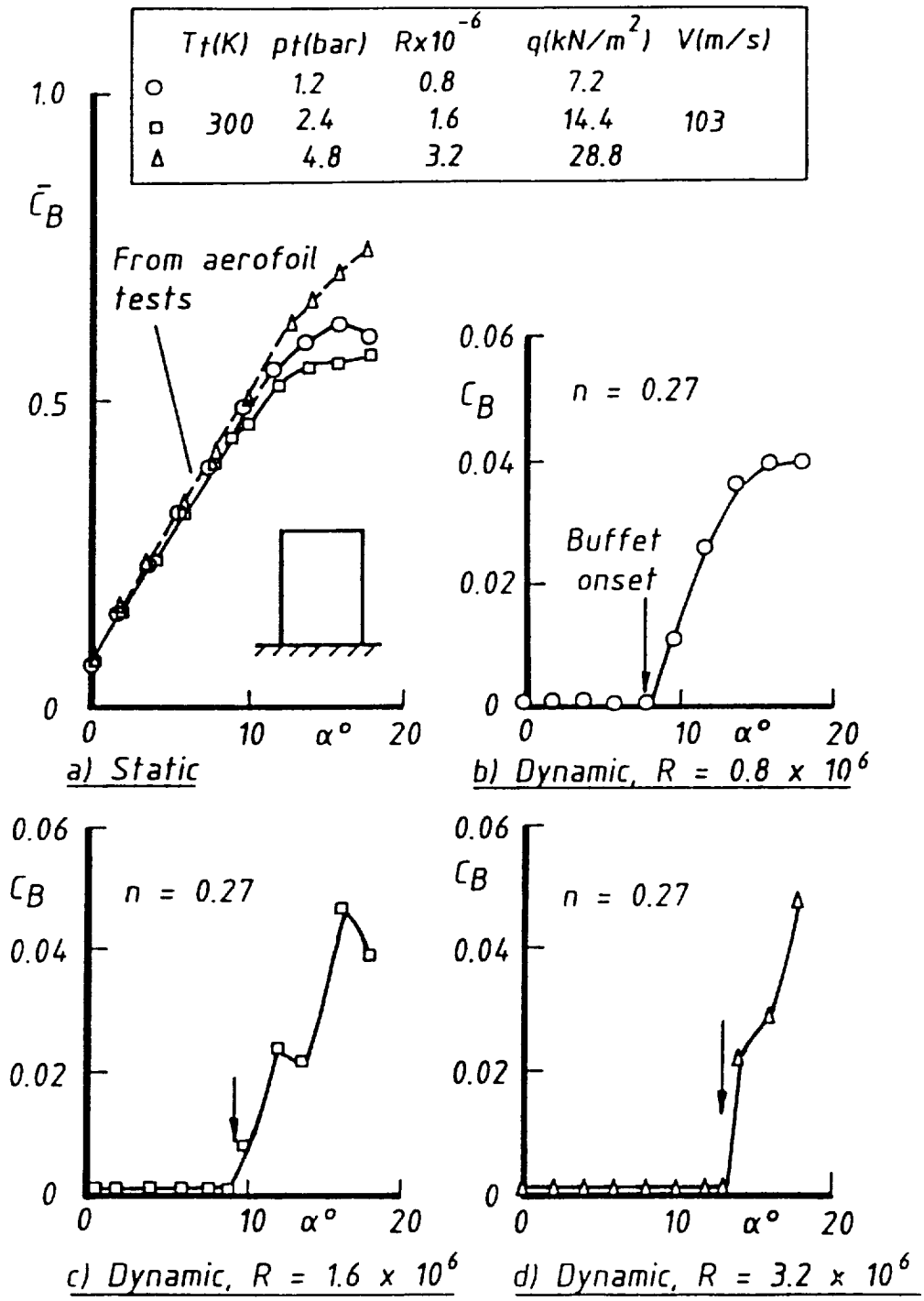

Fig 11 Tests at ambient total temperature on unswept wing

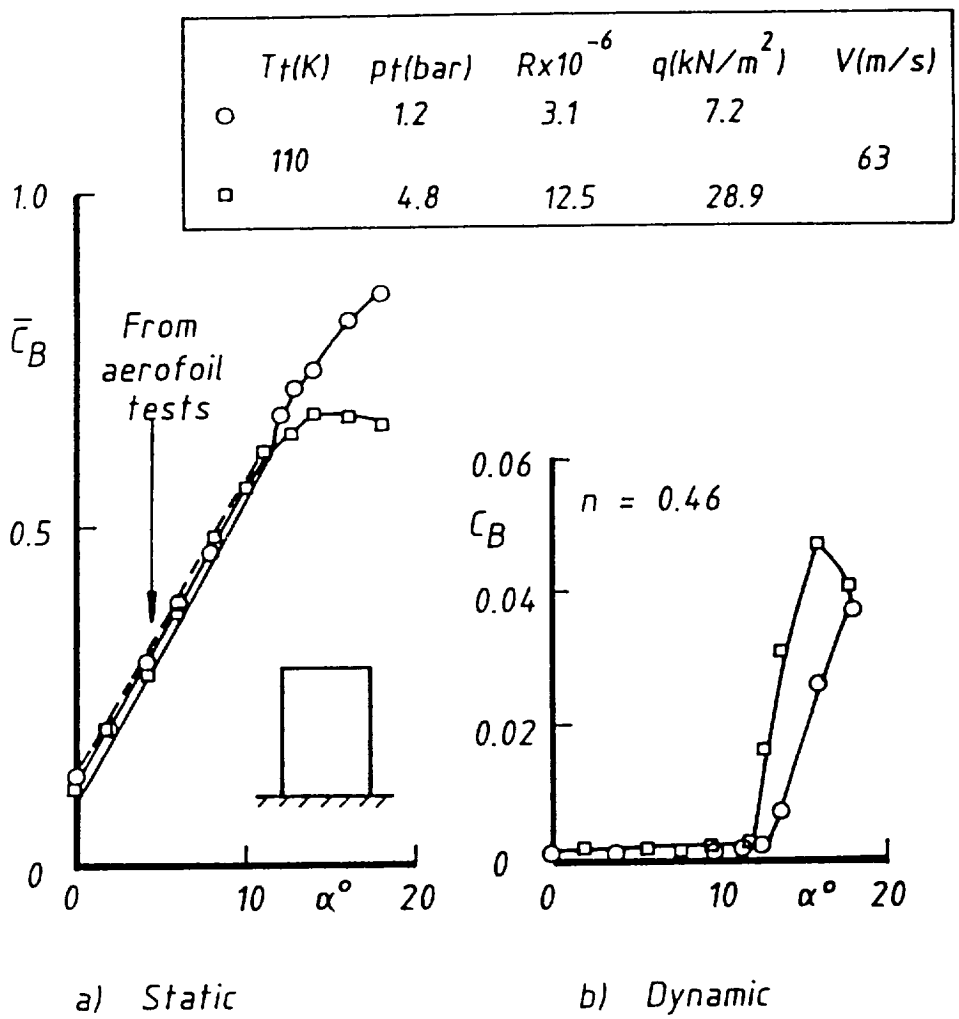

Fig 12 Tests at T_t = 110 K on unswept wing

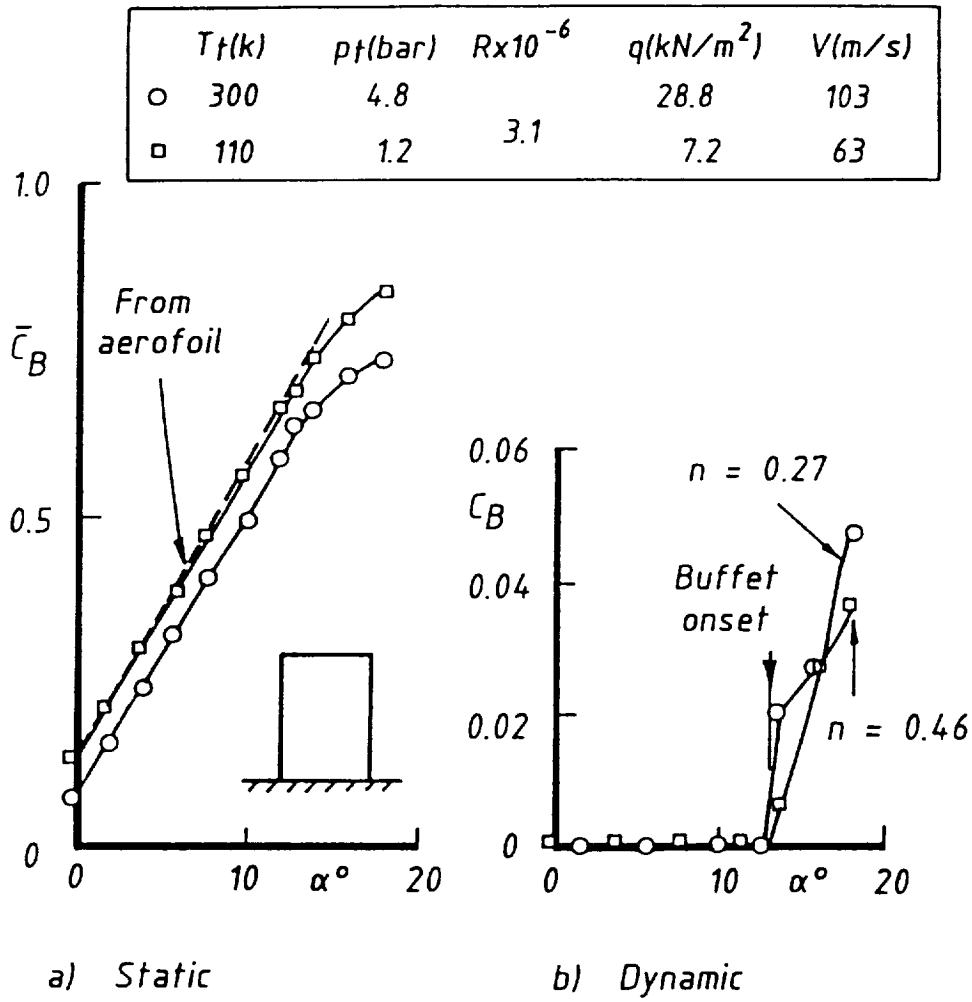

Fig 13 Tests at constant Reynolds number and Mach number (M = 0.30)

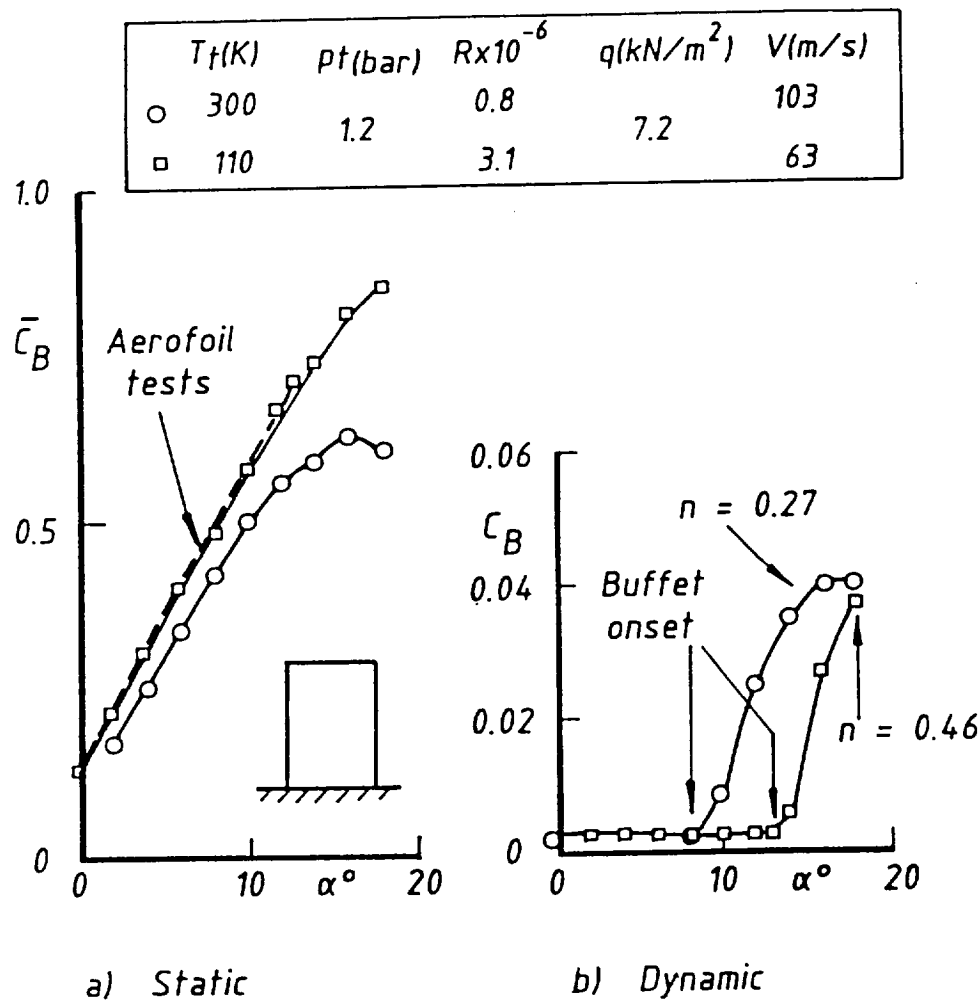

Fig 14 Tests at low kinetic pressure and Mach number (M = 0.30)

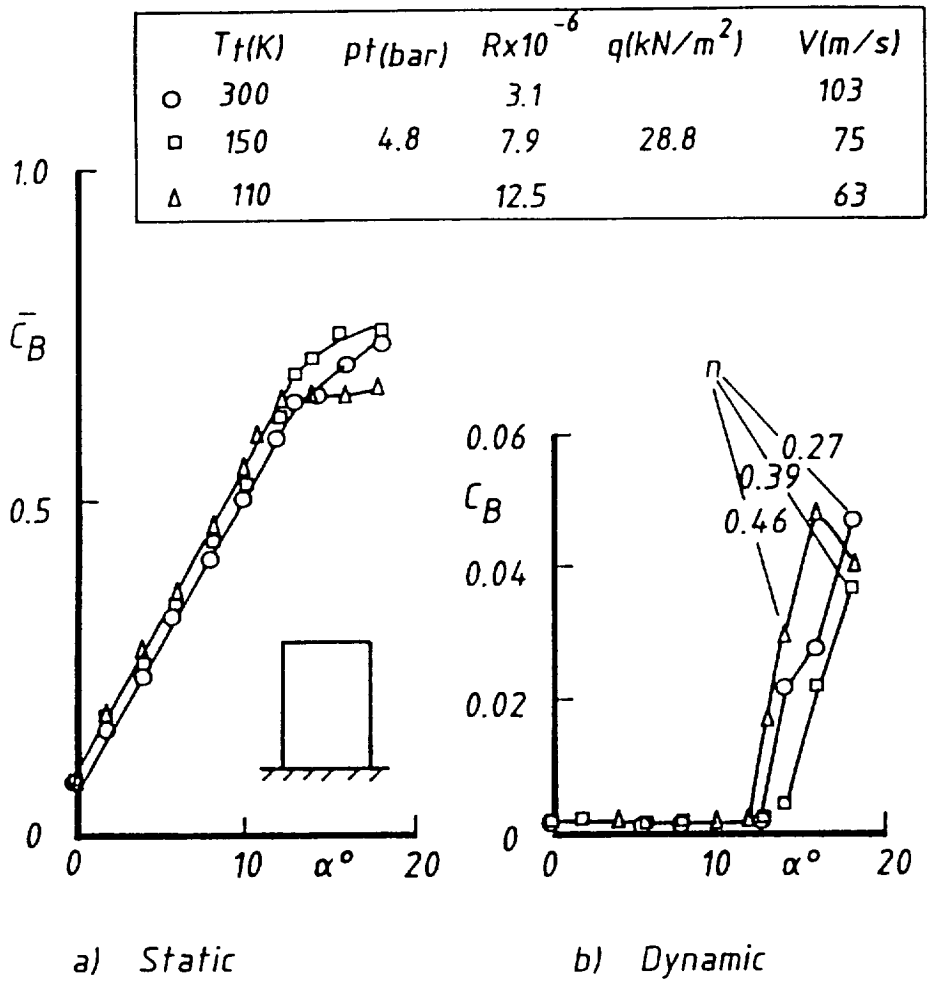

Fig 15 Tests at high kinetic pressure and constant Mach number

	M	Tt(K)	pt(bar)	$Rx10^{-6}$	$q(kN/m^2)$	V(m/s)
○	0.3			3.1	7.2	63
□	0.6	110	1.2	5.6	24.0	122
×	0.7			6.3	30.1	140
Δ	0.8			6.3	35.7	158

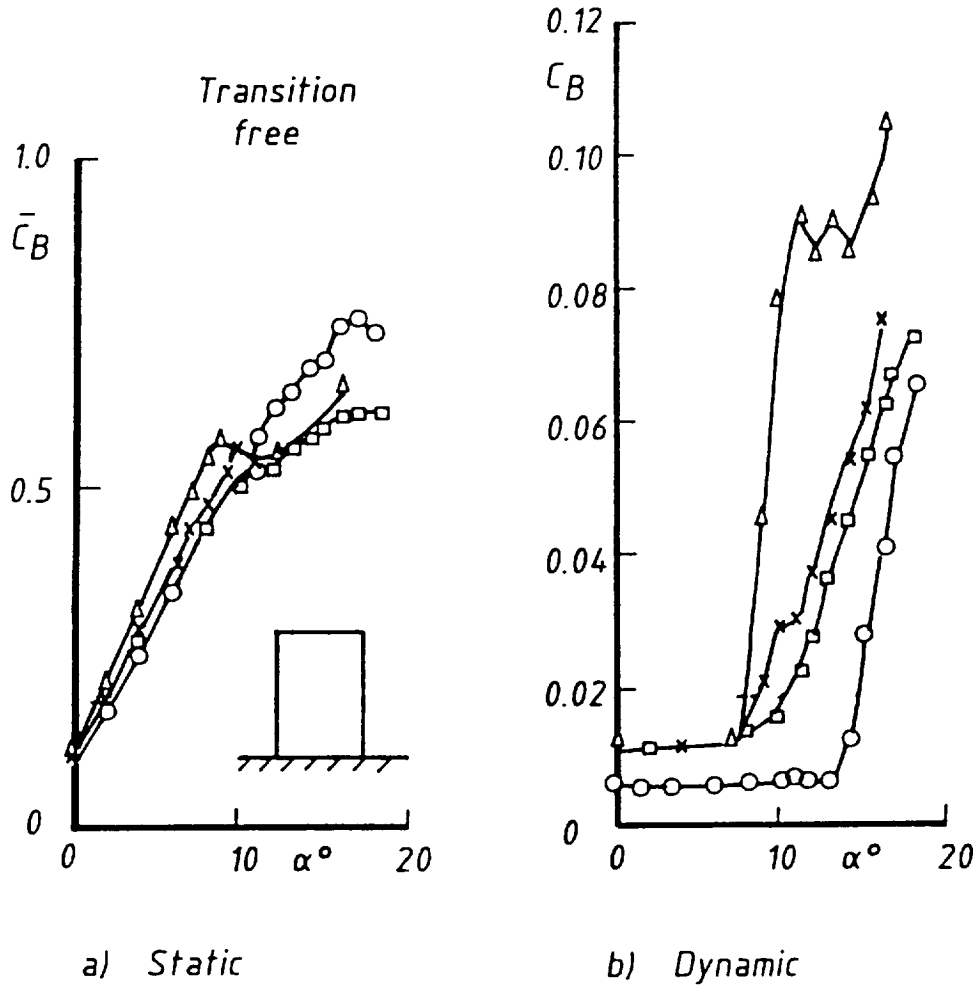

Fig 16 Influence of Mach number on unswept wing (after Ref 4)

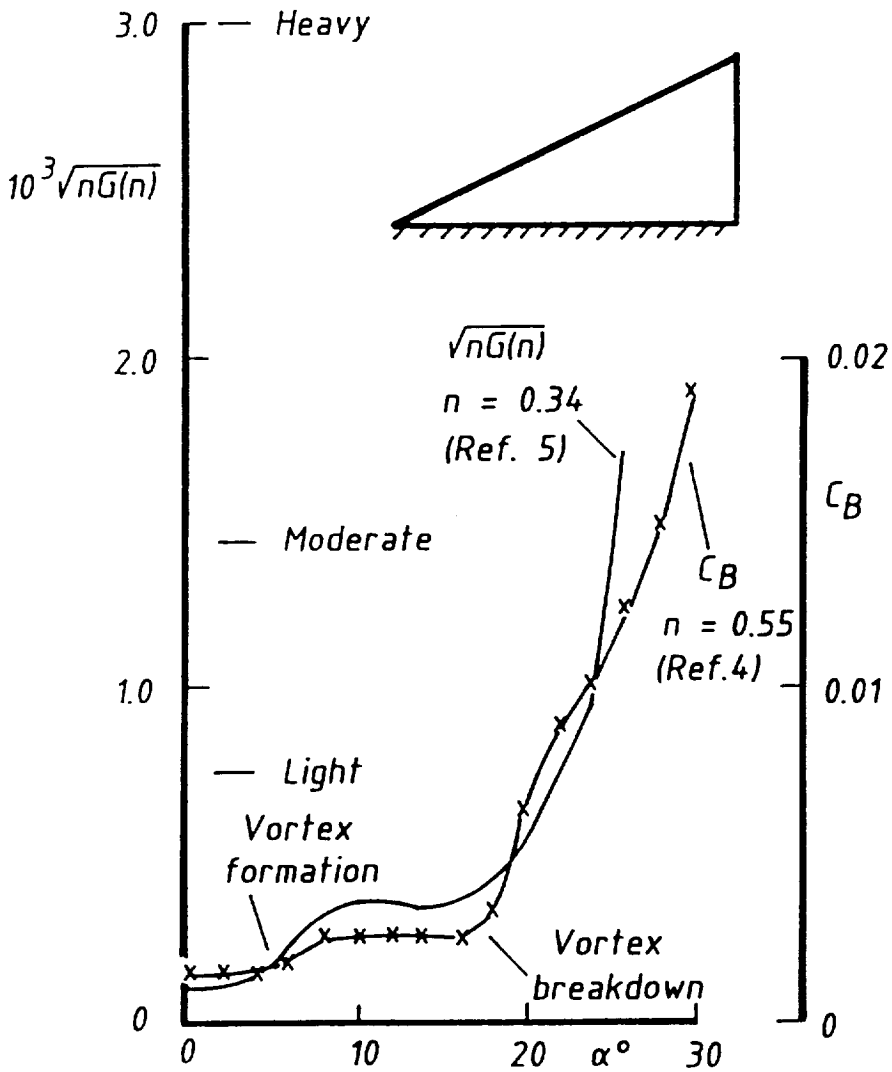

Fig 17 Comparison of buffeting measurements on delta wings in two different wind tunnels

Fig 18

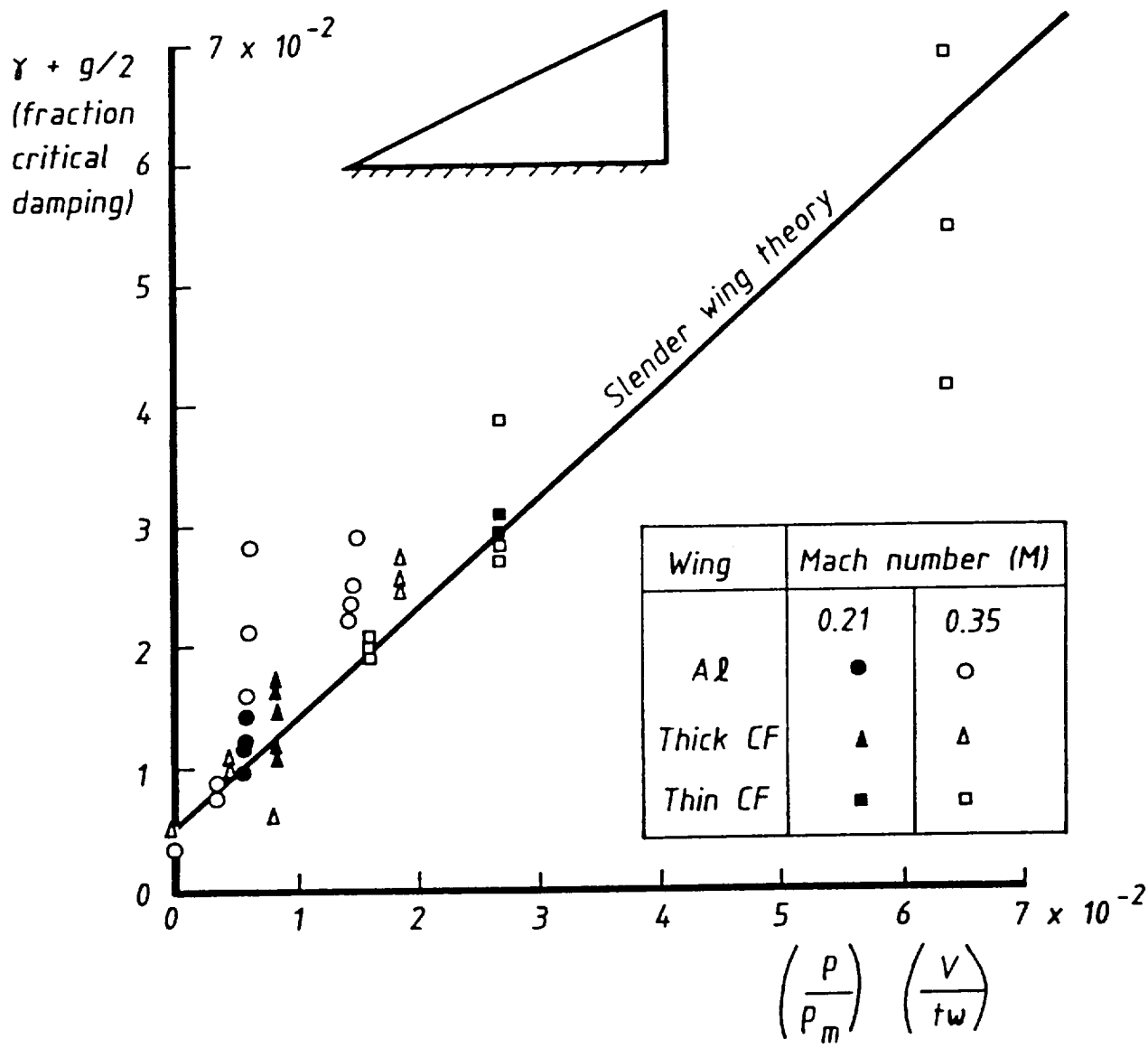

Fig 18 Comparison of estimated and measured total damping for delta wings

REPORT DOCUMENTATION PAGE

Form Approved
OMB No. 0704-0188

1. AGENCY USE ONLY (Leave blank)	2. REPORT DATE	3. REPORT TYPE AND DATES COVERED
	September 1992	Technical Memorandum

4. TITLE AND SUBTITLE

Further Buffeting Tests in a Cryogenic Wind Tunnel

5. FUNDING NUMBERS

WU 505-59-30-01

6. AUTHOR(S)

D. G. Mabey, R. P. Boyden, and W. G. Johnson, Jr.

7. PERFORMING ORGANIZATION NAME(S) AND ADDRESS(ES)

NASA Langley Research Center
Hampton, VA 23665-5225

8. PERFORMING ORGANIZATION REPORT NUMBER

9. SPONSORING/MONITORING AGENCY NAME(S) AND ADDRESS(ES)

National Aeronautics and Space Administration
Langley Research Center
Hampton, Va 23665-5225

10. SPONSORING/MONITORING AGENCY REPORT NUMBER

NASA TM-107621

11. SUPPLEMENTARY NOTES

Mabey: RAE, Bedford, England; Boyden and Johnson: NASA Langley Research Center.
This report was also published as RAE Technical Memorandum Aero 2231.

12a. DISTRIBUTION/AVAILABILITY STATEMENT

Unclassified - Unlimited

Subject Category 02

12b. DISTRIBUTION CODE

13. ABSTRACT *(Maximum 200 words)*

Further measurements of buffeting, using wing-root strain gauges, were made in the NASA Langley 0.3m Cryogenic Wind Tunnel to refine techniques which will be used in larger cryogenic facilities such as the United States National Transonic Facility (NTF) and European Transonic Wind Tunnel (ETW). The questions addressed included the relative importance of variations in frequency parameter and Reynolds number, the choice of model material (considering both stiffness and damping) and the effects of static aeroelastic distortion.

The main series of tests was made on half models of slender 65° delta wings with a sharp leading edge. The three delta wings had the same planform but widely different bending stiffness and frequencies (obtained by varying both the material and the thickness of the wings). It was known that the flow on this configuration would be insensitive to variations in Reynold number.

Additional tests were made on one unswept half-wing of aspect ratio 1.5 with an NPL 9510 aerofoil section, known to be sensitive to variations in Reynolds number at transonic speeds. For brevity the test Mach numbers were restricted to M = 0.21 and 0.35 for the delta wings and to M = 0.30 for the unswept wing.

14. SUBJECT TERMS

Buffet tests
Cryogenic Wind Tunnel
Unsteady Aerodynamics

15. NUMBER OF PAGES

55

16. PRICE CODE

A04

17. SECURITY CLASSIFICATION OF REPORT	18. SECURITY CLASSIFICATION OF THIS PAGE	19. SECURITY CLASSIFICATION OF ABSTRACT	20. LIMITATION OF ABSTRACT
Unclassified	Unclassified		